"In presenting the dissertation as a partial fulfillment of the requirements for an advanced degree from the Georgia Institute of Technology, I agree that the Library of the Institution shall make it available for inspection and circulation in accordance with its regulations governing materials of this type. I agree that permission to copy from, or to publish from, this dissertation may be granted by the professor under whose direction it was written, or, in his absence, by the dean of the Graduate Division when such copying or publication is solely for scholarly purposes and does not involve potential financial gain. It is understood that any copying from, or publication of, this dissertation which involves potential financial gain will not be allowed without written permission.

_____

PREDICTOR CONTROL OF A POSITIONING SERVOMECHANISM

A THESIS

Presented to

the Faculty of the Graduate Division

by

Robert Clinton Carden, III

In Partial Fulfillment

of the Requirements for the Degree

Master of Science

in the School of Electrical Engineering

Georgia Institute of Technology

August 1959

PREDICTOR CONTROL OF A POSITIONING

SERVOMECHANISM

Approved:

Thesis Advisor

Date Approved by Chairman: Aug 30, 1959

ACKNOWLEDGMENTS

I am indebted to Professor
John Milton Bailey for
suggesting this topic and
for his many contributions.

TABLE OF CONTENTS

Page

SYMBOLS

Upper Case, Latin

$E_b = K_b c'$	Motor generated voltage	volts
E_p	Power supply no-load voltage	volts
F	Restoring force	lbs.
$G = \frac{1}{R}$	Equivalent shunt conductance	mhos
I_a	Motor armature current	amp.
J	Polar moment of inertia referred to the output shaft	lb.ft.^2
K_b	Motor generated voltage constant referred to the output shaft	$\frac{\text{volt sec.}}{\text{rad.}}$
K_d	Tachometer generated voltage constant referred to the output shaft	$\frac{\text{volt sec.}}{\text{rad.}}$
K_T	Motor torque constant referred to output shaft	$\frac{\text{lb.ft.}}{\text{amp.}}$
K_x	Recorder x-axis scale factor	$\frac{\text{in.}}{\text{rad.}}$
K_y	Recorder y-axis scale factor	$\frac{\text{in.sec.}}{\text{rad.}}$

$R = R_p + R_s + R_d + R_a$	Series resistance, armature circuit	ohms
R_a	Brush, interpole, and winding resistance	ohms
R_d	Added resistance	ohms
R_p	Power supply resistance	ohms
R_s	Series field resistance	ohms
T	Equivalent applied torque referred to the output shaft	lb.ft.
T_F	Dry friction torque referred to the output shaft	lb.ft.
V_a	Function generator input voltage	volts
V_b	Function generator output voltage	volts

Lower Case, Latin

c	Angular position of the output shaft	rad.
$e = r - c$	System error function	rad.
f	Total viscous coefficient	$\frac{\text{lb.ft.sec.}}{\text{rad.}}$
g	Nonlinear operator	

$k = v + u$	Dimensionless forcing function	
n	Motor to output shaft gear ratio	
$p = \frac{t}{q}$	Dimensionless time	
$q = \frac{J}{f}$	Time constant of the servomechanism	sec.
r	Angular position of the input shaft	rad.
s	Laplace Transform complex variable	
sgn	Signum (sign of)	
t	Real time	sec.
$u = \begin{cases} +1 \\ 0 \\ -1 \end{cases}$	Dimensionless predictor switch function	
$v = \frac{v_i}{v_s}$	Dimensionless input velocity	
v_i	Input velocity	$\frac{\text{rad.}}{\text{sec.}}$
$v_s = \frac{T}{f}$	Servomechanism saturation velocity	$\frac{\text{rad.}}{\text{sec.}}$
$x = \frac{e}{qv_s}$	Dimensionless error	
$'$	First derivative operator	
$''$	Second derivative operator	

Greek

α	Any function of x and x'	
β	Any other function of x and x'	
Δ	Increment of	
γ	Viscous coefficient of friction referred to the output shaft	$\frac{\text{lb.ft.sec.}}{\text{rad.}}$
$\lambda = \pm F$	Elementary contactor control function	lbs.
π	3.14159	
$\Upsilon = K_{\Upsilon} I_a$	Motor developed torque referred to the output shaft	lb.ft.

LIST OF TABLES

LIST OF ILLUSTRATIONS

ABSTRACT

PREDICTOR CONTROL OF A POSITIONING SERVOMECHANISM

Robert Clinton Carden, III

Advisor: John Milton Bailey

A new method of optimizing the response of a second order contactor servomechanism has been investigated. The differential equations of motion of a servomechanism which include the effects of inertia and viscous damping have been solved and transformed into the phase plane. By the use of the phase plane, a relation has been obtained between the error and the error time derivative which exists when optimum switching occurs. This relation describes the boundary in the phase plane where the corrective torque must be reversed if optimum response is to result. Optimum response is characterized by the simultaneous reduction of the error and the error derivative to minimum and zero respectively.

A laboratory model which utilizes this boundary for switching was constructed and its response recorded when subjected to displacement errors. These errors were introduced (1) with the output shaft stationary and (2) with the output shaft in motion. The corresponding responses were computed using the solutions to the assumed differential equations of motion. A comparison was made between the observed and computed responses. The observed responses were found to be within ten per cent of the computed responses for both conditions (1) and (2).

The responses of the predictor servomechanism described above have also been compared with the responses of an uncompensated equivalent contactor servomechanism where the switching is dependent on error polarity. The predictor system displays optimum response for a range of displacement errors from 4 to 24 radians magnitude for both conditions (1) and (2). The uncompensated system response varies with the magnitude of the error and is not optimum.

The predictor system performance was found to be adversely affected by any variance of the dynamic parameters. A system is needed which will allow these parameters to vary with time. A simplified design procedure for higher ordered systems is also needed, since the phase plane is useful for representing only second and lower ordered systems.

CHAPTER I

INTRODUCTION

Statement of the problem.--The response of a discontinuous or "contactor" servomechanism is to be optimized.

In continuous servomechanisms the corrective force is continuously applied to the load as long as an error exists. In a special case of the linear continuous system the corrective force is completely dependent upon the error in both magnitude and polarity. This "proportional error" system has been extensively exploited in theory and practice (1), (2).

The contactor servomechanism, in contrast, utilizes a fixed-magnitude corrective force, so that there is no proportionality between the error and the corrective force. The only means of control are, then, the polarity of the corrective force and the choice of time during which a given polarity will act. In many contactor systems (e.g., thermostat heat controls) the polarity of the correction is changed when the error variable changes polarity. These systems behave awkwardly when subjected to sudden input demands (as when a new desired temperature is dialed at the thermostat). The resulting response is either underdamped (oscillatory) or overdamped (sluggish) according to the magnitude of the input demand. These systems seldom realize their inherent ability to reduce the error in minimum time.

To solve these problems associated with contactor systems, this paper discusses a new method of control whereby the error derivative as

well as the error determines the polarity of the correction. The error and the error derivative indicate the respective potential and kinetic energies stored in the system at any time. Thus, in this system, at any time these quantities along with known unvarying dynamics are used to predict future corrective action. The polarity reversal (switching) occurs automatically at the predicted time to allow the response to be optimum for any magnitude of input demand. The ability of a control system to predict future corrective action and to act at the predicted time characterizes a relatively new concept in servomechanism theory, predictor control, which is the object of this study.

Method of attack.--The equations of motion of a contactor servomechanism--specifically, the rotational positioning type--are studied. The relationship which exists between the error and error derivative when optimum response occurs is determined. In this discussion optimum response is characterized by the reduction of the transient error and error derivative to zero in minimum time. In addition, "optimum response" will imply the transient error and the error derivative are reduced to zero simultaneously for any pair of initial conditions.

This relationship is then used to derive the predictor method of control, which is incorporated into a laboratory model so that the theoretical and physical systems can be compared. The response of the laboratory predictor system to step-displacement inputs is then observed. The observed response is compared with the theoretical response. A comparison is also made between the predictor system and an equivalent uncompensated contactor system.

History of predictor control.--The development of discontinuous automatic control has advanced rapidly in recent years through the use of the mathematical phase plane and nonlinear analysis. In the formulative years of control theory early writers recognized the potential of discontinuous systems. Hazen (3), in 1934, discussed discontinuous automatic control along with the continuous type and pointed out the merits of each. For the next eleven years linear (continuous) control systems dominated the literature, probably because of their amenity to conventional linear methods of analysis. However, during these years DeJuhasz (4) successfully used the phase plane in the analysis of nonlinear processes and instruments, as did Minorsky (5) in the study of parametrically excited circuits.

Meanwhile in Russia, nonlinear analysis had gained new prominence, in 1937, with the publication of The Theory of Oscillations by Andronow and Chaikin (6).

In 1945, MacColl (7) applied the phase plane to the study of an ideal contactor servomechanism with a finite inactive zone where switching was dependent upon error polarity. In the same year Weiss (8) used the phase plane to develop the transient and steady-state analysis of a rotational system with intermittently applied torque. The analysis included the effects of inertia, viscous and dry friction, finite inactive zone, and constant delay time in torque change. Weiss also discussed compensation techniques to eliminate steady-state oscillation caused by the rotation of the switching boundary in the phase plane. The rotation was attributed to the combined effects of inactive zone and time delay. Among these techniques was lead stabilization (derivative compensation)

which rotated the boundary in the opposite sense to counteract the oscillatory tendency. In this paper Weiss recommends lead stabilization as "the most logical damping device to be applied to a high performance relay servomechanism." Rotation of the linear switching boundary in the phase plane by the use of derivative compensation is the basis of predictor control today. Linear switching has been exhaustively studied by Flugge-Lotz (9).

The concept of a linear switch boundary in the phase plane suggested the use of a curved boundary. This was investigated by MacDonald (10) who inroduced nonlinear lead networks for the optimization of a second order system. The curvature of the switch locus was made to conform to the final trajectory in the phase plane.

Hopkin (11) applied this technique to a realistic system and discussed the implementation of the curved switching boundary by experimental means. Since the publication of these works, predictor control theory has been extended considerably. Discussions of third and higher order systems as well as dual-mode predictor systems are available (12), (13).

This study is based on the cited works of Weiss, MacDonald, and Hopkin and attempts to utilize their theories in order to realize a physical system by "engineering method"--i.e., analysis, design, experimental observation, and comparison with theoretical promise. It is expected that the methods presented here will be helpful in the design of practical predictor systems.

CHAPTER II

PRELIMINARY CONSIDERATIONS

Contactor positioning systems.--A servomechanism is a device which establishes a functional relationship between an input or reference variable $r(t)$ and an output or controlled variable $c(t)$. Furthermore, the energy supplied to the output is not furnished directly from the input but is derived from a separate source.

Such a system, in which the input and output signals represent coordinates in space so that the position of the output member is a function of the position of the input member, is referred to as a positioning servomechanism. If the input and output members are mechanical systems with one degree of freedom, their motion can be completely described by the respective variables $r(t)$ and $c(t)$. The ideal functional relation for a servomechanism is an exact correspondence between input and output,

$$c(t) = r(t) \ . \tag{1}$$

Since the static accuracy of any control system is limited, (1) cannot physically occur. In addition, the energy storage elements prevent $c(t)$ from following rapid variations in $r(t)$. To account for these undesirable effects, the system error function $e(t)$ is introduced so that

$$c(t) = r(t) - e(t) \ . \tag{2}$$

In this equation, e(t) contains a transient component resulting from the energy storage and a constant component resulting from the system resolution.

After a disturbance, the control system should bring the output c(t) to equal the input r(t) to within specified limits of static error e(t) in minimum time. That is, the system must transfer energy to the output in the form of a corrective force. This force can be applied either continuously or discontinuously. The proportional-error control is an example of continuous application of corrective force, the force varying linearly with the system error. In contrast a discontinuous control utilizes only a few discrete values of corrective force applied in turn until the transient error vanishes.

To reduce the transient system error to zero in minimum time, the full available corrective force should be applied during the transient period. Linear systems, by nature, do not operate at the saturation level; consequently only a small per cent of the available corrective force is used. Linear systems are thus characterized by wasted energy capacity and the associated bulky motivating units.

This disadvantage is overcome to an extent in a discontinuous control (hereafter called a contactor control) in which the corrective force is switched between two oppositely polarized values, $\pm$ F.

An elementary contactor system is shown in Fig. 1. The corrective force changes sign with the system error function e(t) so that

$$\lambda(e) = + F \qquad e(t) > 0$$

and (3)

$$\lambda(e) = - F \qquad e(t) < 0$$

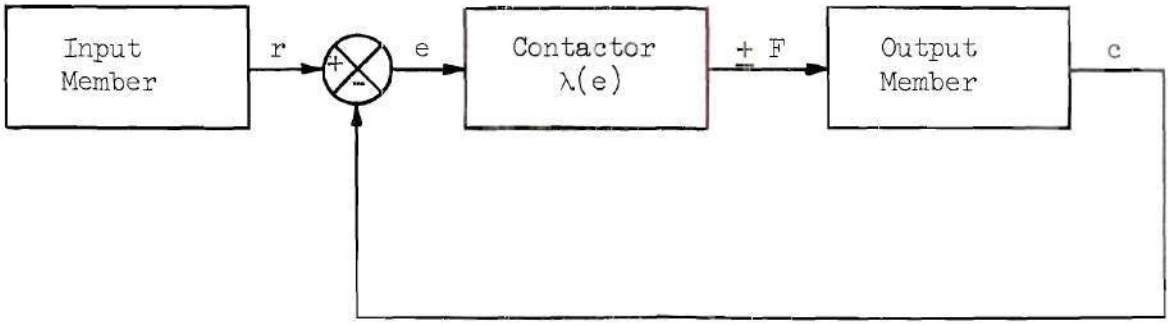

Fig. 1 Elementary Contactor System, Block Diagram

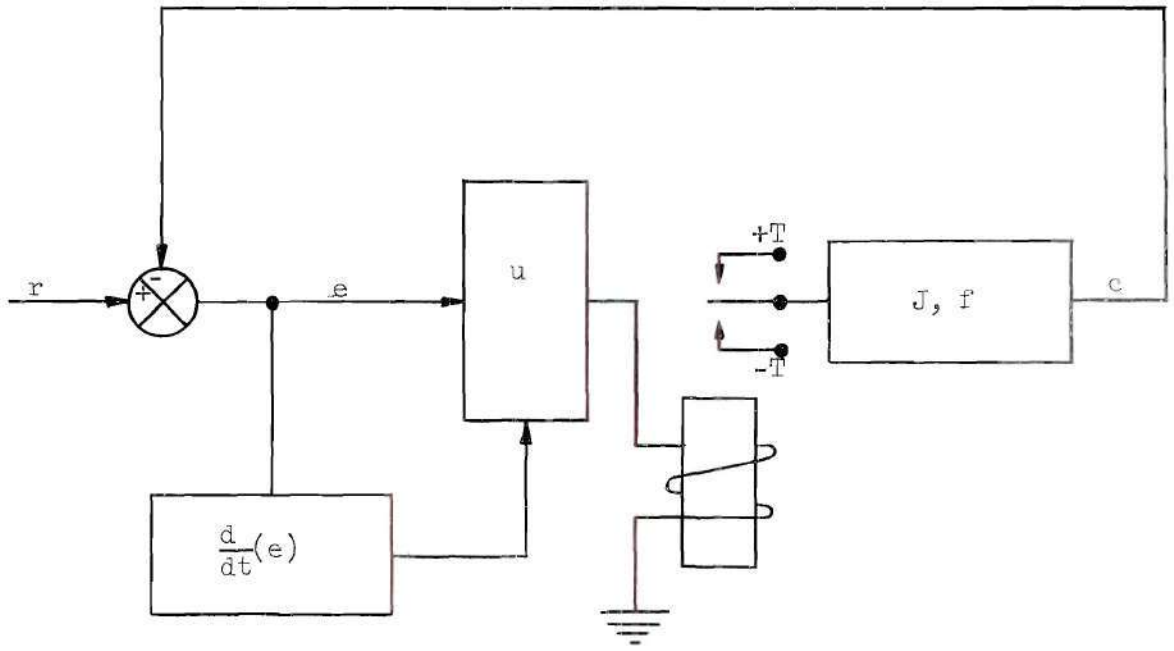

Fig. 2 Predictor Control System, Block Diagram

Here no mention is made of the neighborhood of e = 0. In this region, however small, F = 0 so that the system "coasts" force-free during a portion of each transition period. It is apparent that this zone must exist if steady-state oscillation is prohibited. The effects of this so-called inactive zone will be considered later, but for the present system they are taken as negligibly small.

The response of this contactor system (Fig. 1) is plotted in Fig. 3-a where a step displacement (r=1.00) is assumed. The limitations of this elementary system stem from the many reversals required for each correction and the resulting underdamped response. If the initial overshoot (1.28) of Fig. 3-a cannot be tolerated, the damping can be adjusted to give a minimum time response for this displacement; however, the response to larger displacements will be correspondingly overdamped.

The discussion so far has been concerned with displacement inputs, tacitly assuming no initial velocity of the output member. Actually a design which overlooks the effects of stored kinetic energy is not realistic; a typical case depicted in Fig. 3-b illustrates the effects of initial velocity. Here the system of Fig. 3-a is subject to the same displacement input while its output member is in motion.

The initial velocity in this case causes a larger first overshoot (1.29), so that a larger negative correction interval (0.92 q) is required to dissipate the excessive energy supplied by this initial velocity. Since a large overshoot is usually undesirable, the need arises for anticipating the negative corrective force and applying it earlier in the transient period to obtain a response with the minimum possible overshoot. (If the system were continuous and not oscillatory in the steady state,

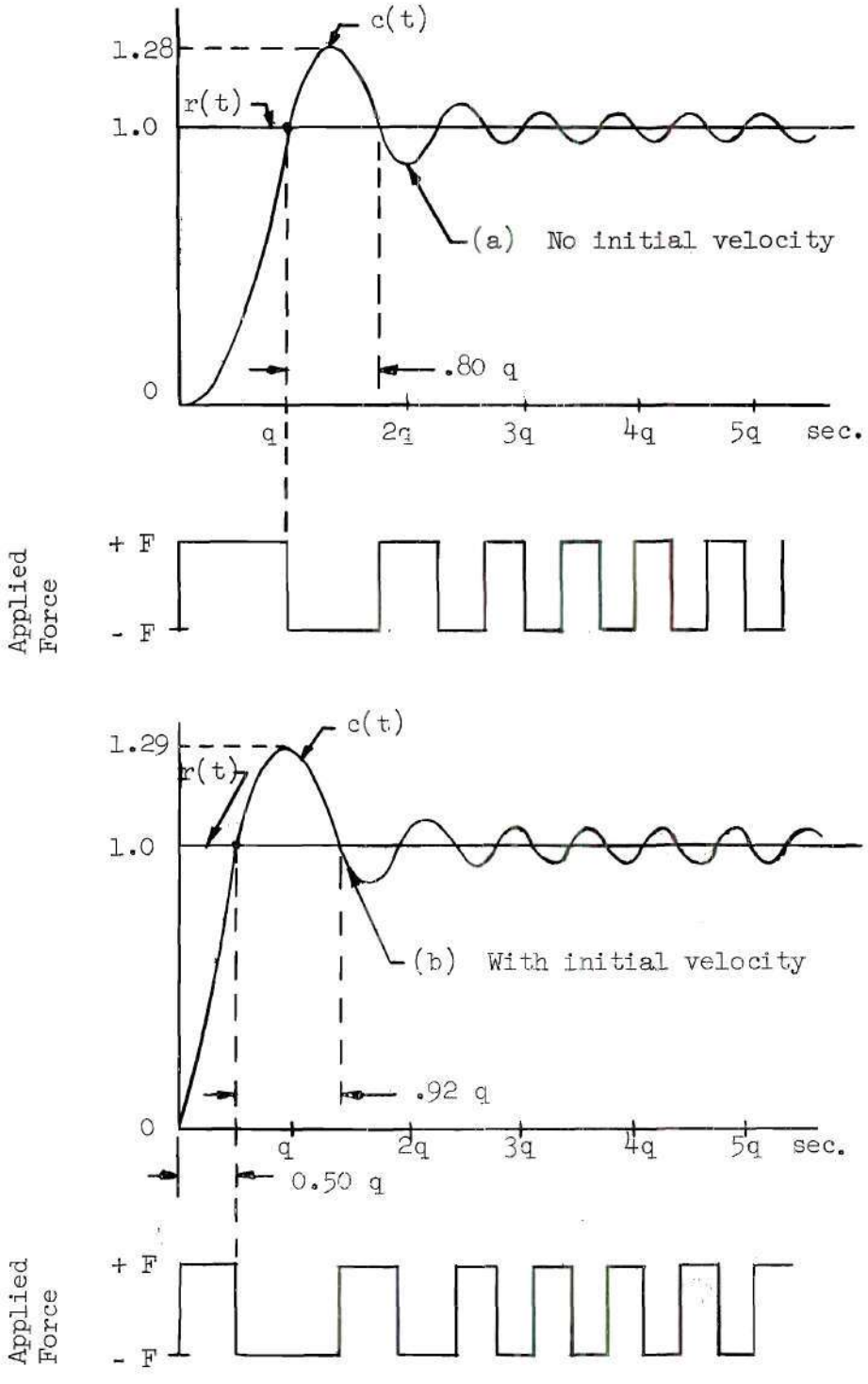

Fig. 3 Elementary Contactor Response with and without Initial Velocity

this response would correspond to a critically damped response.) This concept is pictured in Fig. 4 for the previously discussed input and initial velocity. Here, the polarity of F is not directly dependent upon the polarity of the error function, as is evident from the fact that the error has not changed sign at the first switchpoint (0.40 q). Obviously, different values of input displacement and initial output velocity will require different instants at which this force reversal should take place. To be operative for more than one pair of initial conditions, the system of Fig. 4 must be capable of predicting the switching instant required for any combination of initial error and initial velocity.

A system which responds in the manner of Fig. 4 has been made realizable through a powerful method of analysis known as the phase plane. The system to be described, providing an optimum response for any set of input displacements and initial velocity, is known as a "Predictor Controller."

Phase plane analysis.--As pointed out by Truxal (14), the phase plane analysis is used in the study of systems having a wide variety of nonlinearities. These systems can be described by the equation,

$$x'' + \alpha x' + \beta x = 0 \qquad (4)$$

where the primes indicate differentiation with respect to the independent variable, time. Coefficients α and β can be functions of x and x' but not of time explicitly. The forcing function of the system is restricted to be constant or linear with time. The phase plane, a rectangular plot of x' against x, for a typical control system is shown in Fig. 5. The initial conditions,

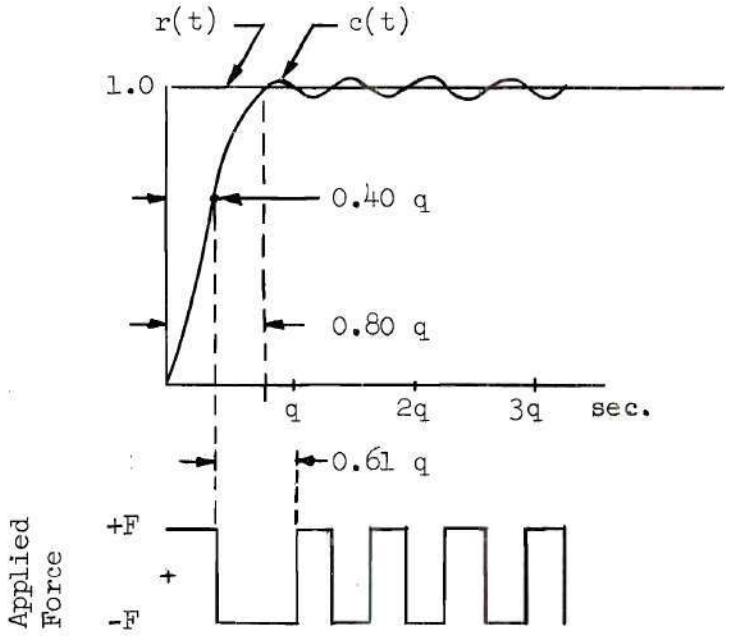

Fig. 4 Predictor Contactor Response with Initial Velocity

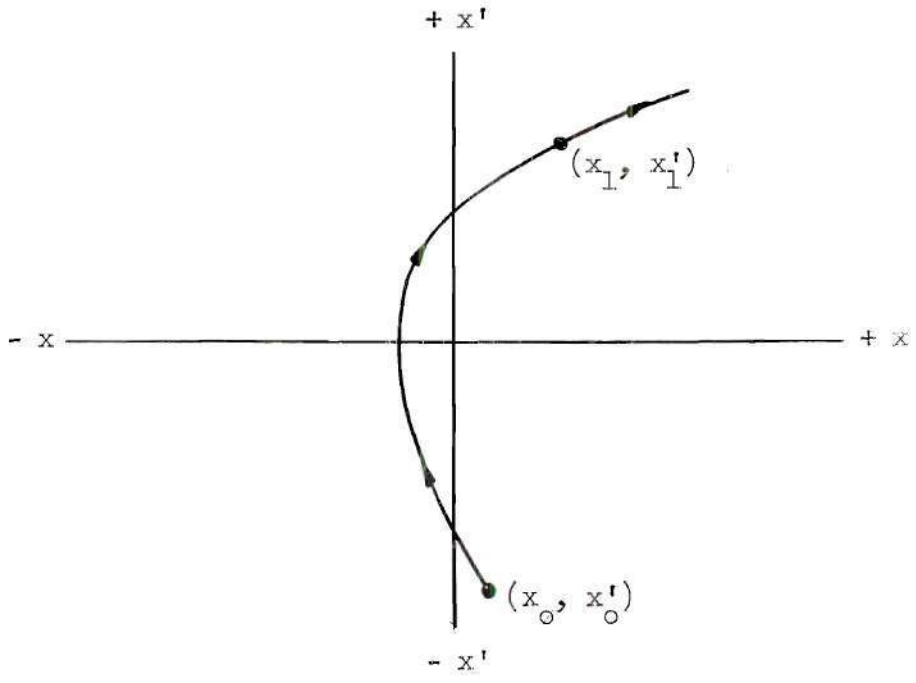

Fig. 5 Phase Plane Trajectory

$$x_o = x(0^+)$$
$$x_o' = x'(0^+) \tag{5}$$

are the coordinates at time $t = 0^+$. Since the initial conditions define a unique solution to the equation represented on the phase plane, the path through (x_o, x_o') describes the behavior of the system at all later times. This path is called the trajectory. Since the trajectory through (x_o, x_o') is unique, there can be no other through (x_o, x_o') as long as the phase plane represents only one differential equation. Since there can be only one path through (x_o, x_o'), there can be no intersections in the phase plane, for any point (x, x') could be considered as the initial coordinate pair, (x_o, x_o').

If the describing equation in linear, an equilibrium point, or singular point, exists at the origin. A stable linear system has all of its paths converging on the origin, whereas the unstable system trajectories diverge from the origin, approaching infinity.

Furthermore, trajectories in the upper half-plane are directed to the right and in the lower half-plane, to the left. This statement follows from the relation

$$\frac{dx}{dt} = x' \tag{6}$$

which states that x increases with time when $x' > 0$ and decreases when $x' < 0$.

Although not explicitly evident from the phase plane plot, time may be computed analytically or graphically in the following manner:

Observing that

$$x' = \frac{dx}{dt} \tag{6}$$

then

$$dt = (\frac{1}{x'})dx$$

and

$$t_1 = \int_{x_o}^{x_1} (\frac{1}{x'})dx \ . \tag{7}$$

The elapsed time between any two points in the phase plane is the area under the inverse velocity curve plotted against x.

The significance of the slope in the plane is found by dividing the acceleration,

$$x'' = \frac{d(x')}{dt} \tag{8}$$

by the velocity, x', so that

$$\frac{x''}{x'} = \frac{\frac{d(x')}{dt}}{\frac{dx}{dt}} = \frac{d(x')}{dx}$$

which can be written,

$$x'' = x' \frac{d(x')}{dx} \ . \tag{9}$$

The acceleration at any point is the product of the velocity and the slope of the trajectory at this point. Consequently, trajectories which cross the abscissa (finite non-zero acceleration) do so perpendicularly, fulfilling (9) with the indeterminate product $(0)(\infty)$ at the abscissa.

The phase plane is restricted in use in that systems analyzed with it must be acting under the constraint of constant or linear forcing functions. Furthermore, the plane is two-dimensional, so that higher order systems must be analyzed in the phase space. Motion which is constrained by sinusoids or periodic functions which are not piecewise linear is more suitably analyzed by another method (15).

Phase plane optimization.--The phase plane of Fig. 6 depicts the correction process of an elementary rotational positioner for the initial conditions, e_o, e'_o.

For convenience the error, instead of the output angle, is plotted in the phase diagram. The points at which the corrective torque is switched are labeled consecutively. The switch points are located at the boundaries of the inactive zone. The intervals of free motion in the inactive zone appear as straight line trajectories. The torque removal and reversal continue until the system comes to rest in the inactive zone. Weiss (16) has shown that performance can be improved by adjusting the switch boundary in the plane so that the initial switch point is located earlier along the trajectory. As MacDonald (17) demonstrated, the boundary can also be distorted to conform with the decelerating path, thereby realizing optimum response. Rotation of the switch boundary is implemented by using the error derivative as well as the error

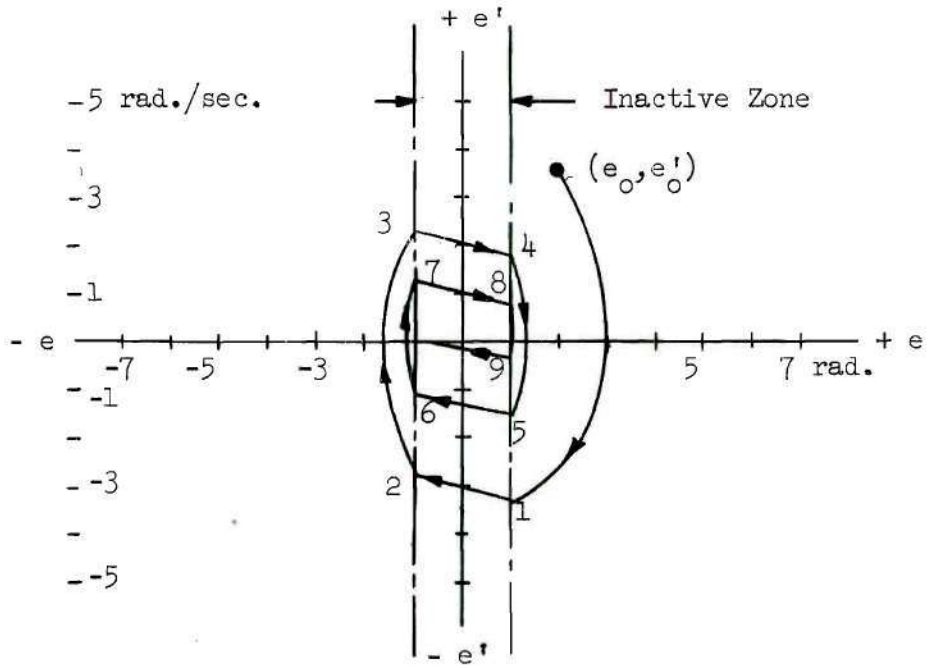

Fig. 6 Switch Boundaries, No Compensation

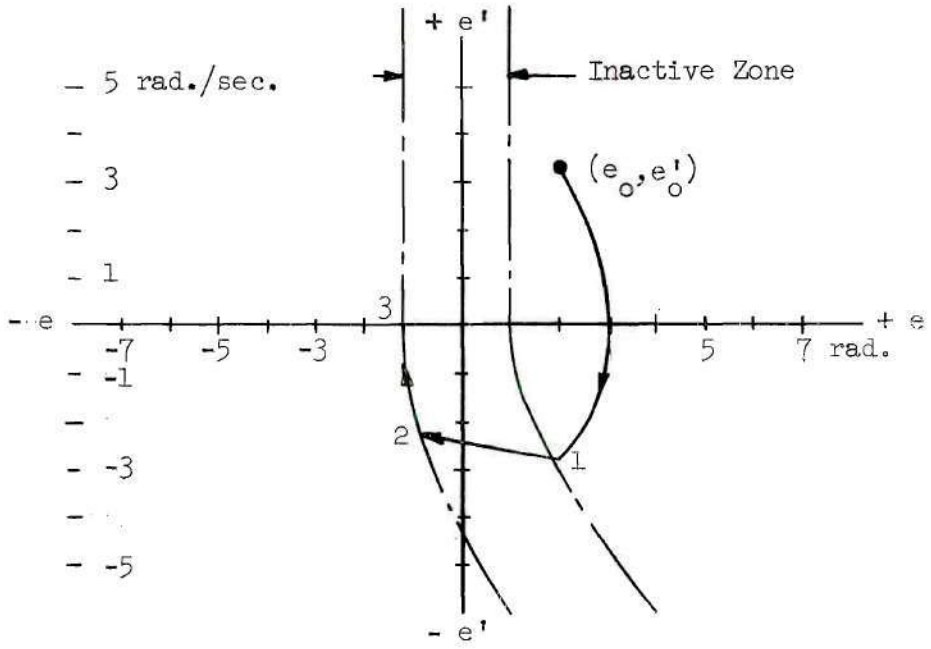

Fig. 7 Switch Boundaries Modified by Nonlinear Derivative Compensation in the Lower Half-plane

to control the relay. The derivative signal is then modified by a non-linear element. These methods are illustrated in Fig. 7 and are the distinguishing features of the predictor controller of Fig. 2. The choice of the switch function u will be made evident by solving the equations of motion and transforming the solutions to the phase plane.

CHAPTER III

SYNTHESIS OF THE SYSTEM

Solution of the equations of motion.--The following detailed development of the phase plane trajectories from the differential equation of motion follows the one outlined by Weiss (18). The system to be considered is a rotational positioner with inertial and viscous loading and instantaneously applied torque.

The equation of motion of the system in Fig. 2 is

$$Jc'' + fc' = - Tu \tag{10}$$

where c is a function of time, and the forcing function is either + T, - T, or 0, according to the function u which is to be derived. Divide this equation through by f and substitute v_s and q into (10). Thus,

$$qc'' + c' = - v_s u \ . \tag{11}$$

For a displacement or constant velocity input, r'' = 0, so that the derivatives of the error function, e, will have the form,

$$e' = v_i - c' \tag{12}$$

and

$$e'' = - c'' \ . \tag{13}$$

Using (12) and (13) to eliminate c in (11) results in the error equation,

$$qe'' + e' = v_i + v_s u \tag{14}$$

which after dividing through by v_s and substituting v into (14) gives

$$\frac{q}{v_s} e'' + \frac{1}{v_s} e' = v + u \ . \tag{15}$$

To introduce p in place of t in (15) first derive e'(p) and e"(p) by noting that

$$t = qp \tag{16}$$

and

$$e'(p) = \frac{de(t)}{dp} = \left(\frac{de}{dt}\right)\left(\frac{dt}{dp}\right) \ .$$

Then,

$$e'(p) = q \frac{de}{dt} \ . \tag{17}$$

In similar manner

$$e''(p) = \frac{d}{dt} \left(q \frac{de}{dt}\right) \frac{dt}{dp}$$

which reduces to

$$e''(p) = q^2 \frac{de^2}{dt^2} \ . \tag{18}$$

Substitute (17) and (18) into (15) observing that the primes now indicate differentiation with respect to p. Thus (15) becomes

$$\frac{1}{qv_s} e'' + \frac{1}{qv_s} e' = v + u \ . \tag{19}$$

The dimensionless error function x is now introduced by differentiating x and substituting for e in (19), which reduces to

$$x'' + x' = v + u \ . \tag{20}$$

The discontinuous function u prevents the possibility of a general solution to (20); however, in a particular switched state the right hand side of (20) is constant so that, excluding switch transients,

$$x'' + x' = k \tag{21}$$

where k is a real number.

Apply the Laplace transformation to (21) to obtain

$$s^2 x(s) - s x_o - x_o' + s x(s) - x_o = \frac{k}{s} \ .$$

Extracting x(s), and expanding,

$$x(s) = \left[\frac{k}{s} + x_o' \right] \left[\frac{1}{s} - \frac{1}{s+1} \right] + \frac{x_o}{s} \ .$$

The inverse transform is

$$x(p) = k \int_o^p (1 - e^{-p}) dp + x_o'(1 - e^{-p}) + x_o$$

in which

$$k \int_{o}^{p} (1 - e^{-p})dp = k\,[p - (1 - e^{-p})] \ .$$

The solution in the time domain is then

$$x(p) = k\,p - (k - x_o')(1 - e^{-p}) + x_o \tag{22}$$

which after differentiation yields

$$x'(p) = k - (k - x_o')e^{-p} \ . \tag{23}$$

Equations (22) and (23) will now be solved simultaneously for x and x', eliminating p. Noting that from (23)

$$e^{-p} = \frac{k - x'}{k - x_o'} \tag{24}$$

and

$$p = \ln\left[\frac{k - x_o'}{k - x'}\right] \tag{25}$$

which when substituted into (22) will eliminate p. Thus,

$$\frac{x}{k} - \frac{x_o}{k} = \ln\left[\frac{1 - \frac{x_o'}{k}}{1 - \frac{x'}{k}}\right] - \frac{x'}{k} + \frac{x_o'}{k} \ . \tag{26}$$

The phase plane representation of (26) is given in Fig. 8. Curves opening to the right (dashed) describe motion when $k > 0$, and curves opening

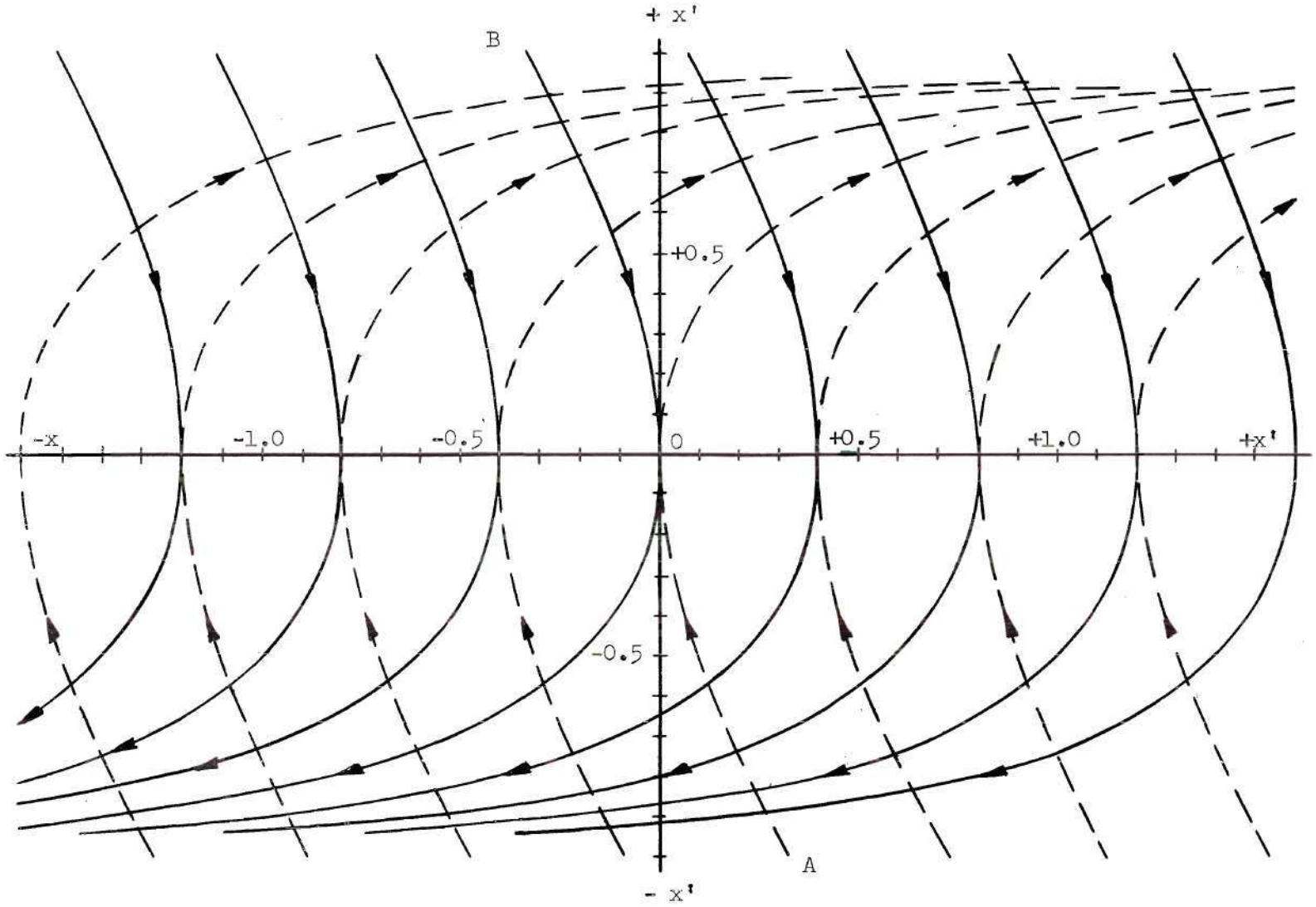

Fig. 8 Phase Plane Representation, Equation (26)

to the left (solid) are for $k < 0$. Of special interest are the trajectories described by (26), which pass through the origin. By assuming $x_o = 0$ and $x'_o = 0$, (26) reduces to

$$\frac{x}{k} + \frac{x'}{k} + \ln\left(1 - \frac{x'}{k}\right) = 0 \ . \qquad (27)$$

The response to a step-displacement input is found when $v = 0$; then $k = u$ so that

$$k_{(v=0)} = \begin{cases} +1 \\ 0 \\ -1 \end{cases} .$$

Equation (27) under these conditions becomes

$$x + x' + \ln(1 - x') = 0 \qquad (k = 1) \qquad (28)$$

$$x + x' = 0 \qquad (k = 0) \qquad (29)$$

$$x + x' - \ln(1 + x') = 0 \qquad (k = -1) \ . \qquad (30)$$

If (28) is plotted, the resulting curve can be used as a template to plot any of the calculated trajectories. This follows from (26), which states that all trajectories for a particular value of k are identical except for the shifting constant, $\left(\frac{x_o + x'_o}{k}\right)$. The curve for (30) can be obtained from (28) by inverting (28) from left to right and top to bottom. The template curve for (28) is shown in Fig. 9. The coordinates and calculations for this trajectory are given in Tables 3 and 4. All of the calculated phase plane responses were drawn using this template (e.g., Figs. 10, 20, 22, 23).

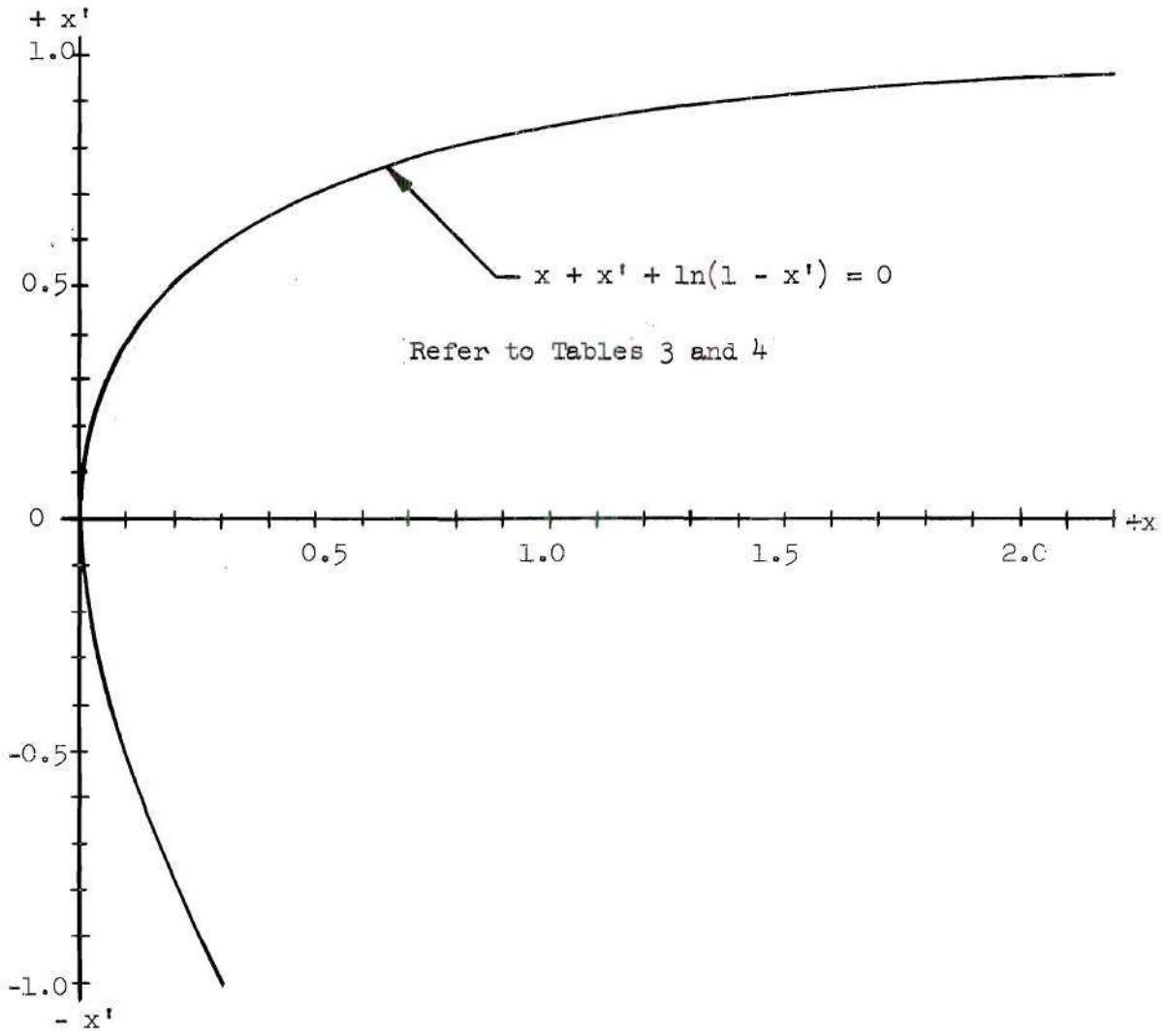

Fig. 9 Open Loop Trajectory, Equation (28)

Switch boundaries, negligible inactive zone.--Assuming for the present discussion that the inactive zone represented by (29) is negligibly small, (28) and (30) can be thought of as the final trajectories during any correction interval. These are deceleration paths representing "critically damped" motion, which is the case when x and x' vanish simultaneously. These lines are also switching boundaries in the phase plane, where torque reversal must occur. Since the origin is the stable point in the plane, paths that diverge from the origin cannot be used as final trajectories; hence, the second quadrant portion of (30) and the fourth quadrant portion of (28) are to be the decelerating paths. Both (28) and (30) under these restrictions are expressed as one equation,

$$x = [\ |x'| - \ln(1 + |x'|)]\ [-\ \mathrm{sgn}(x')]\ . \tag{31}$$

This is represented by line AOB in Fig. 8. The function u must change values along this boundary to effect torque reversal. It is convenient to realize us physically by introducing a new variable, g, so that

$$g(x') = [\ |x'| - \ln(1 + |x'|)]\ [\ \mathrm{sgn}(x')]\ . \tag{32}$$

Rewriting (31) leads to

$$x + g(x') = 0 \tag{33}$$

which states that the switch line is the locus of null output when x and g signals are added algebraically. The function u can now be defined:

$$u(x,\ x') = \begin{cases} 1 & (x + g) < 0 \\ -1 & (x + g) > 0\ . \end{cases} \tag{34}$$

Fig. 10 is the phase plane representation of the system which utilizes (34) as its switching function. This system is only conditionally stable near the origin where steady oscillations of small magnitude will occur. Although this is sometimes desirable in reducing the effects of static friction, excessive contact wear can result.

Switch boundaries, finite inactive zone.--Fig. 11 illustrates the inclusion of an inactive zone in phase plane switching. Now $u(x, x')$ must be written separately for the half planes:

L.H.P.,

$$u(x, x') = \begin{cases} 1 & x + g + a < 0 \\ 0 & -a < x + g < b \\ -1 & x + g - b > 0 \end{cases} \tag{35}$$

U.H.P.,

$$u(x, x') = \begin{cases} 1 & x + g + b < 0 \\ 0 & -b < x + g < a \\ -1 & x + g - a > 0 \end{cases} .$$

The final trajectories intercept the x axis a units from the origin, while the torque-removal boundary intercepts b units from the origin. By allowing $|b| > |a|$, the system comes to rest at $(\pm a, 0)$.

A typical path of motion is shown in Fig. 11 as a result of the initial conditions, (x_o, x'_o). This path may be described by equation (27) for each interval:

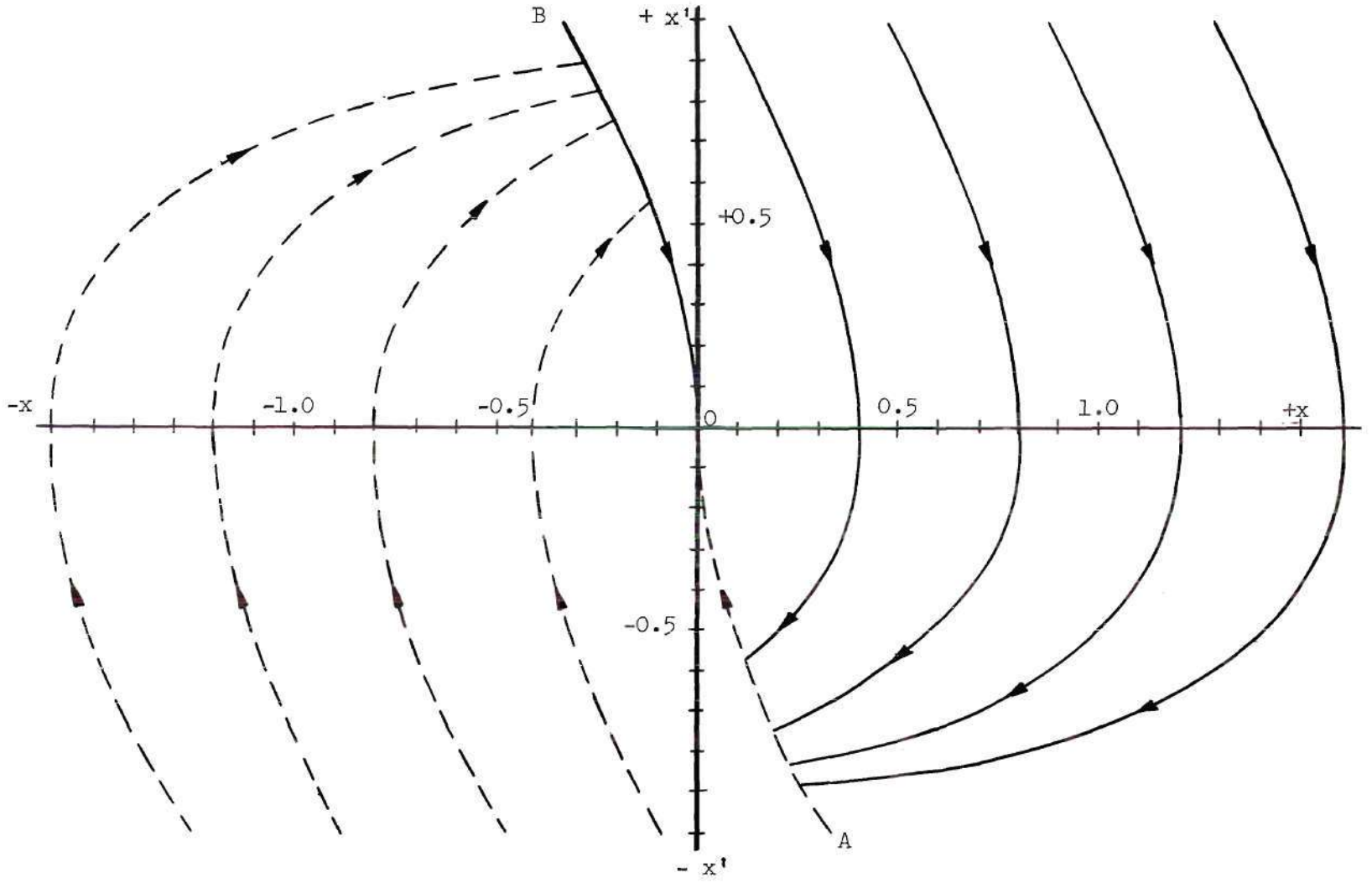

Fig. 10 Trajectories of the System Described by Equation (10) using Equation (34) as the Switch Criterion

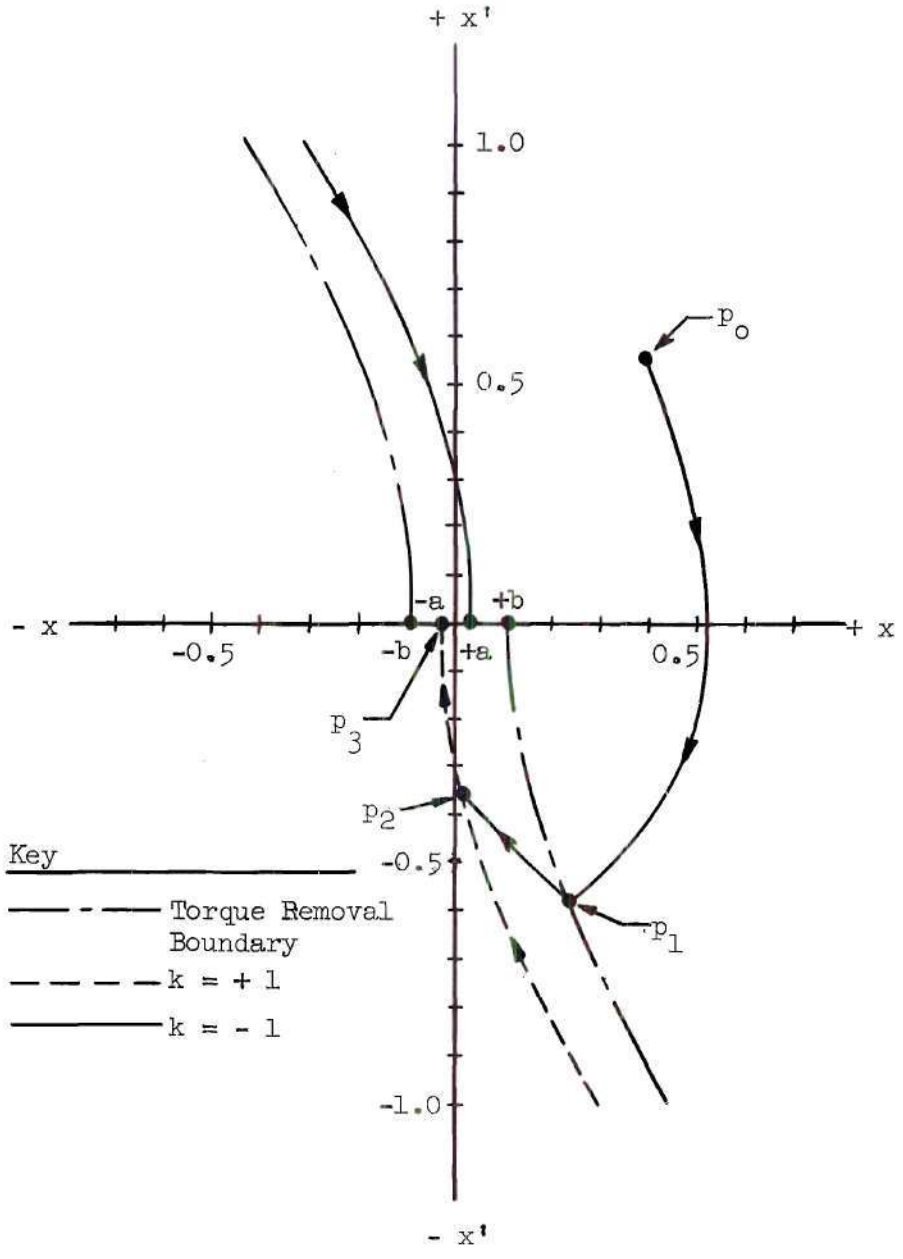

Fig. 11 Modification of the Switch Boundaries to Include an Inactive Zone as Given by Equations (35)

I Acceleration: $k = -1$ $\qquad 0 < p < p_1$

$$x + x' - \ln(x' + 1) = x_o + x_o' - \ln(1 - x_o) \tag{36}$$

II Torque removal: $\qquad p = p_1$

$$x_1 + x_1' + \ln(1 - x_1') = b \tag{37}$$

III "Coasting": $k = 0$ $\qquad p_1 < p < p_2$

$$x - x_1 = (x' - x_1') \tag{38}$$

IV Deceleration: $k = +1$ $\qquad p_2 < p < p_3$

$$x + x' + \ln(1 - x') = -a\ . \tag{39}$$

The response given by (36) through (39) and illustrated in Fig. 11 is optimum for the system under discussion (x and x' are simultaneously reduced to minimum and zero respectively in minimum time). The switch function (35) which yielded this response is therefore used in the laboratory model. The static accuracy using this function is only limited by the value of "a" which can be reduced independently of the inactive zone width (b + a). The magnitude of this zone width depends upon the hysteresis characteristics of the relay and the system gain. For improved time response the zone can be minimized by allowing "b" to be slightly larger than "a" thereby reducing the interval of free motion (38). Experimental adjustment of parameters "a" and "b" is provided for in the laboratory model and is described in Chapter IV.

Implementation of the switch boundaries.--The block diagram of Fig. 12 illustrates the method by which the switch function is incorporated into the laboratory model. The error input to the controller (enclosed by dashed lines) is the difference between the r and c signals from the potentiometers. The error derivative input is supplied by the tachometer at the output shaft, since for displacement inputs, the error derivative is the negative of the output velocity. The g signal is derived from the x' signal as indicated by (32); however, this signal is approximated in the diagram by the output of a nonlinear circuit which modifies the derivative signal. This is a function generator which approximates g(x') by the use of twenty straight segments.

Equation (35) is realized by first establishing the sum of the x and g signals, which yields the switch control function, u. Appropriate biases are then included in the relay drive-circuits to realize the control action of (35). The controller changes the polarity of the armature circuit, thereby changing the torque polarity. During the period of free motion the current source is disconnected, but armature current circulates to maintain dynamic braking.

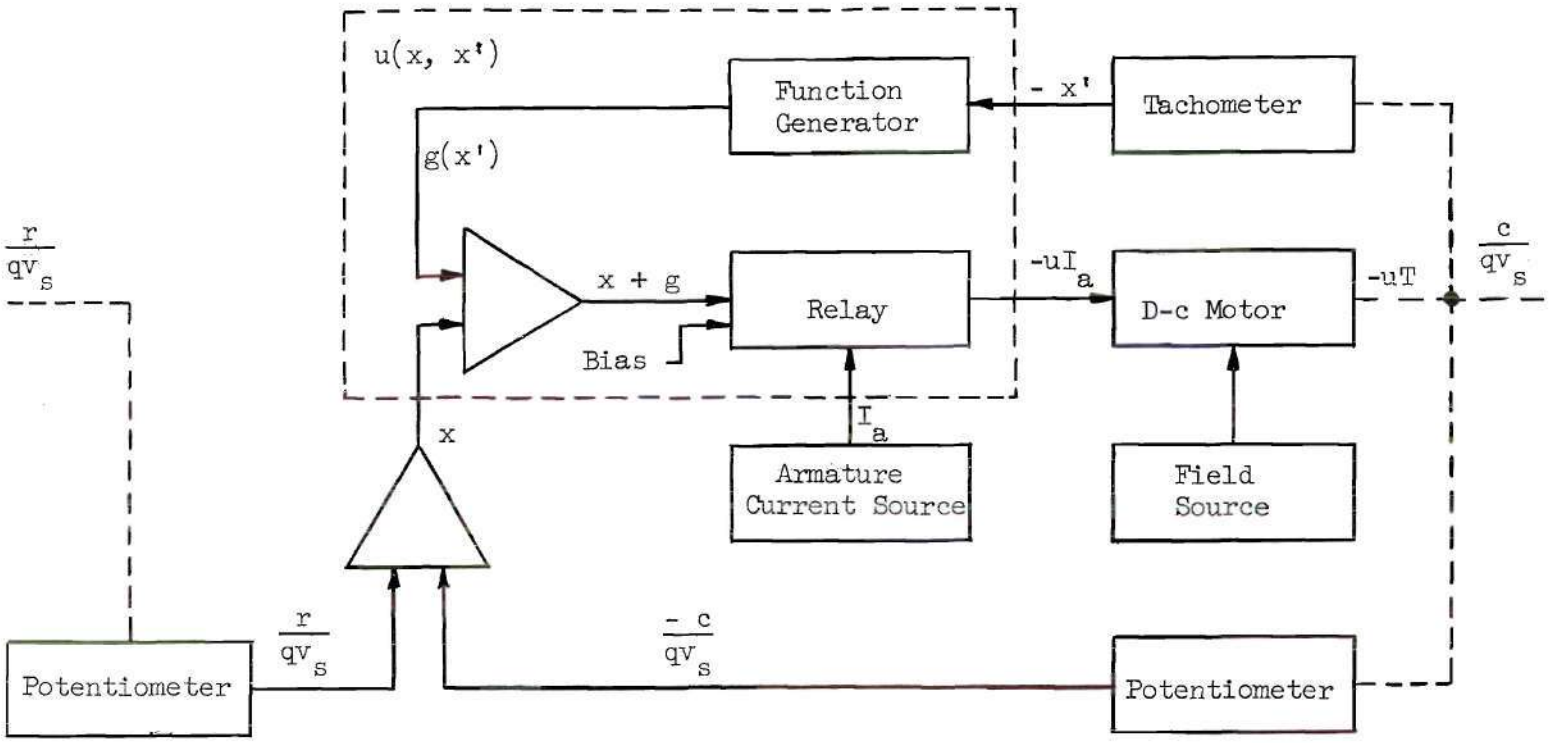

Fig. 12 Simplified Block Diagram of a Predictor Servomechanism

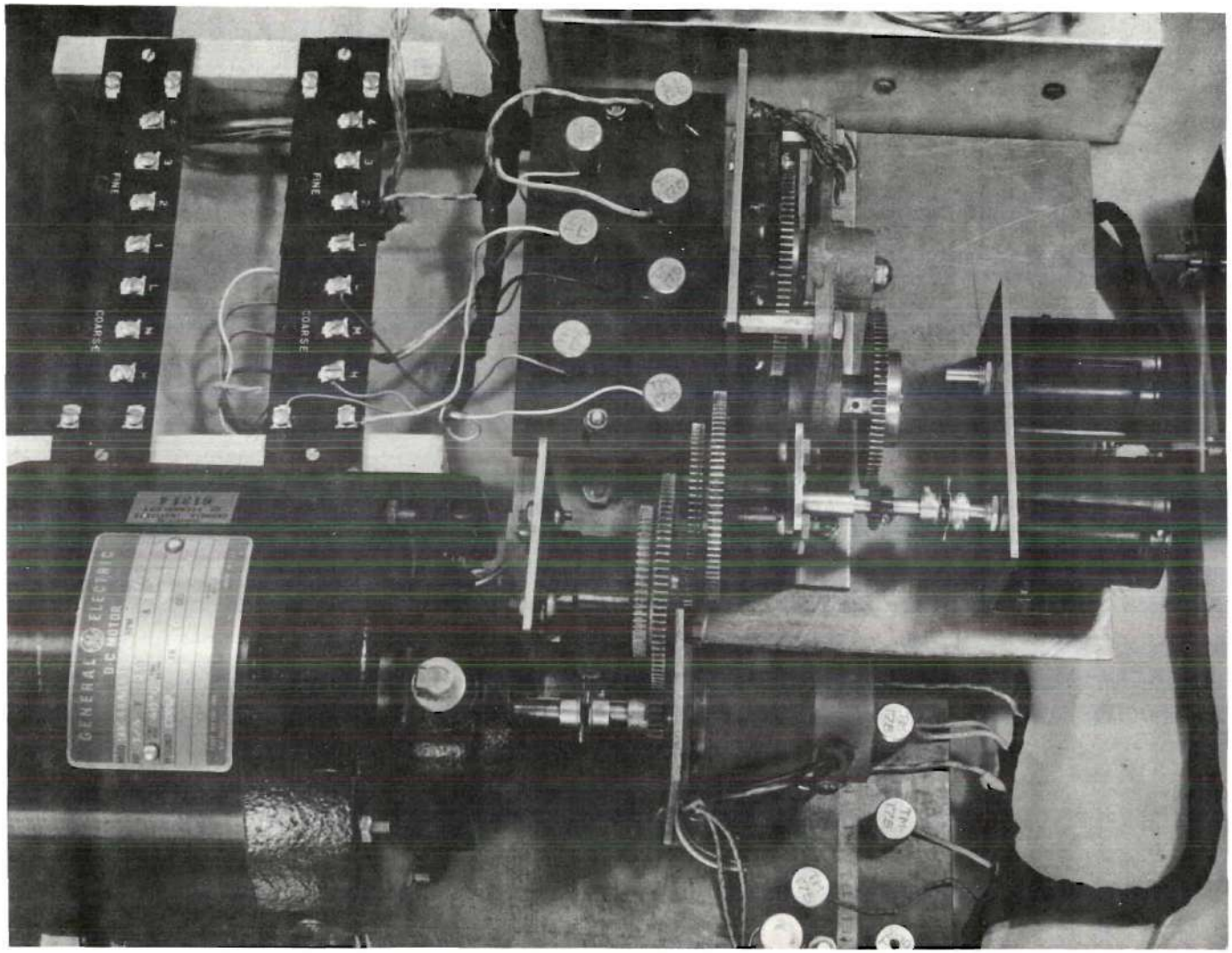

Figure 13. View of the Mechanical Assembly.

CHAPTER IV

REALIZATION OF THE SYSTEM

Method of realization.--A common practice in the design of positional control systems is to utilize a d-c motor as the power element. This practice is due to the ease with which its speed and torque levels can be controlled. For this reason the laboratory model utilizes a one-fourth horsepower d-c motor as its power element. However, the electrical input to such a device is in general a voltage source such as a polyphase rectifier. Since the generated emf of the motor is proportional to speed and presents a varying load to its power source during acceleration, the current changes with speed. Hence, from examination of the torque-current relation for a d-c motor,

$$T = K_T I_a \tag{40}$$

it is seen that if torque is to be switched instantaneously by changing the armature current instantaneously, the driving source must of necessity be an ideal current source. From practical considerations it is more desirable to use a voltage source which is not ideal rather than the ideal current source. Equation (10) can still be realized, however, by including the effect of the generated emf in the viscous coefficient f as demonstrated in Fig. 14. Consider first the system of Fig. 14-a in which the armature circuit of the motor is connected to a laboratory voltage source. The polarity of this voltage source can

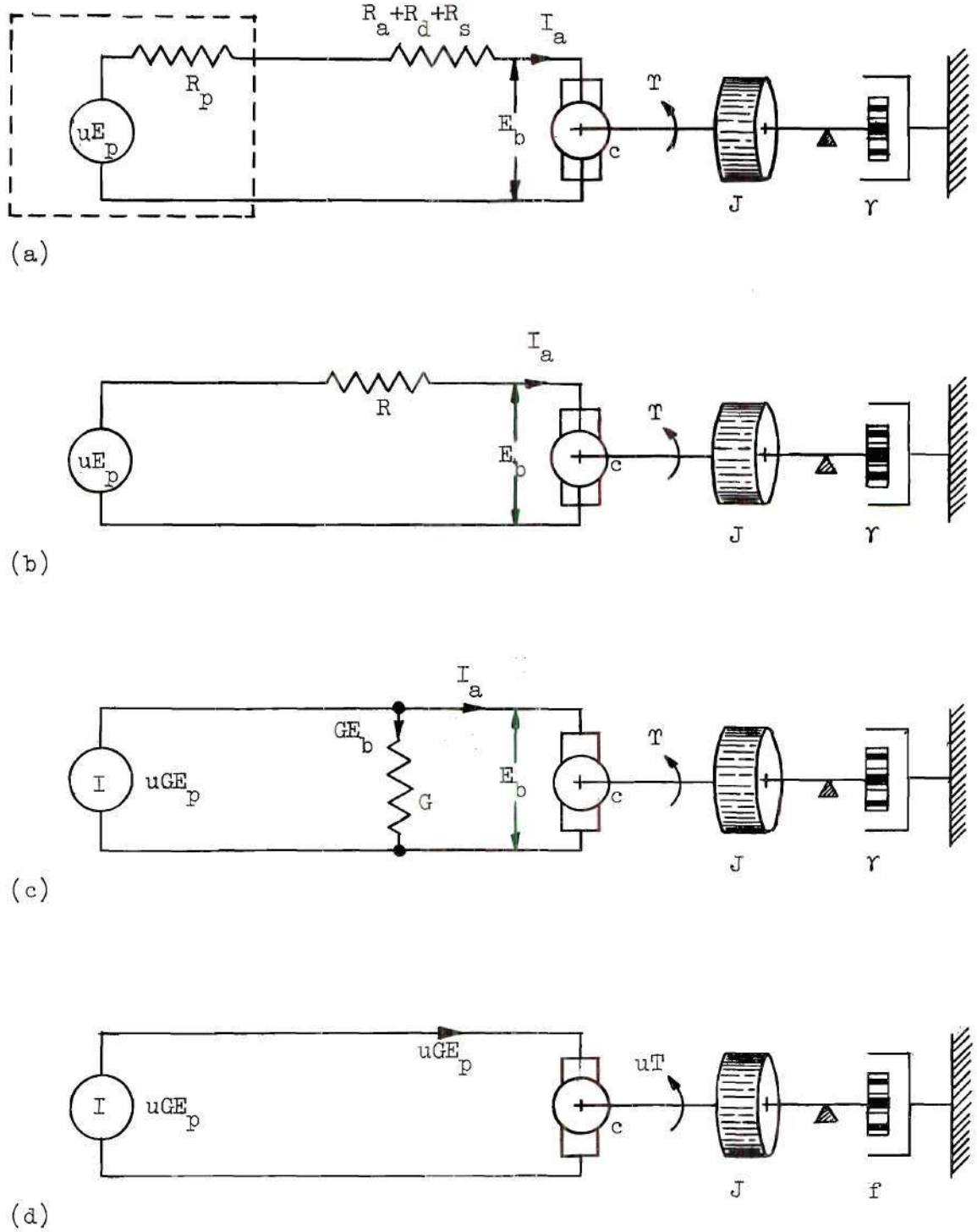

Fig. 14 Equivalent Circuit to Simulate Instantaneous Applied Torque and Adjustable Damping Coefficient

be switched as designated by the term uE_p. The internal resistance of the power supply is denoted R_p, and the resistance external to it, $R_a + R_d + R_s$. The current flowing in the armature causes a torque, T, to be developed which is applied to the load consisting of an inertia J and a viscous damping component γ. The equation of motion is

$$T = Jc'' + \gamma c' \tag{41}$$

which also is true for Fig. 14-b. Fig. 14-b differs from Fig. 14-a only in the substitution of

$$R = (R_a + R_d + R_s) + R_p \ . \tag{42}$$

The Thevinin's equivalent of Fig. 14-b is pictured in Fig. 14-c where

$$G = 1/R \ . \tag{43}$$

The motor generated voltage is designated E_b and is given by the relation

$$E_b = K_b \, c' \ . \tag{44}$$

Kirchhof's current law applied to the upper node in Fig. 14-c yields

$$I_a = uGE_p - GE_b \ . \tag{45}$$

Substitution of (44) into (45) results in

$$I_a = uGE_p - GK_b c' \ . \tag{46}$$

The torque developed may now be expressed from (40) and (46):

$$T = K_T(uGE_p - GK_b c') \ . \tag{47}$$

This equation suggests rewriting the equation of motion (4) in the form,

$$uK_T GE_p = Jc'' + (\gamma + GK_T K_b)c' \tag{48}$$

which defines the following associations:

$$f = \gamma + GK_T K_b \tag{49}$$

and

$$T = K_T GE_p \ . \tag{50}$$

Thus (41) becomes

$$uT = Jc'' + fc' \tag{51}$$

which is a restatement of (10), the equation of motion originally to be realized. The diagram of Fig. 14-d now applies. An instantaneous torque change is obtained by changing E_p instantaneously instead of the armature current. This is easily done by the use of relays. Furthermore, the damping coefficient f can be established by adjusting the parameter G. This adjustment is made by inserting a series variable resistor R_d in the armature circuit. By use of the equivalent diagram Fig. 14-d, the design procedure is readily developed.

Mechanical assembly.--The system proposed in Fig. 12 indicates that the mechanical assembly consists of a motor, an error detecting potentiometer,

and a derivative detecting tachometer. Since the potentiometers are available with only a limited angular span (e.g., 10 revolutions), speed reduction gearing is used between the motor and the output shaft. The speed reduction enables the motor to accelerate and run at near rated values, and allows the plotting devices associated with the output shaft to have considerably slower response characteristics. The inertial load consists of the armature and gear inertia and also the inertia of a flywheel mounted on the motor shaft.

When the power supply, motor, flywheel, and tachometer are assembled, preliminary parameter determinations are made so that the gear train can then be designed. The approximate saturation velocity and the time constant are established neglecting the (small) effect of eventual gear train loading.

The time constant is given by

$$q = \frac{J}{f} = \frac{J}{\gamma + GK_T K_b} \tag{52}$$

where G may be chosen by adjusting a series armature resistance. This choice is made to yield a value for q, which is conveniently displayed on the x-y recorder. Once G has been adjusted to give the desired time constant, the torque T, viscous coefficient f, and the saturation velocity v_s are also established. The expression for the saturation velocity follows from (10) which in the steady state ($c'' = 0$) reduces to

$$c' = v_s = \frac{T}{f} \tag{53}$$

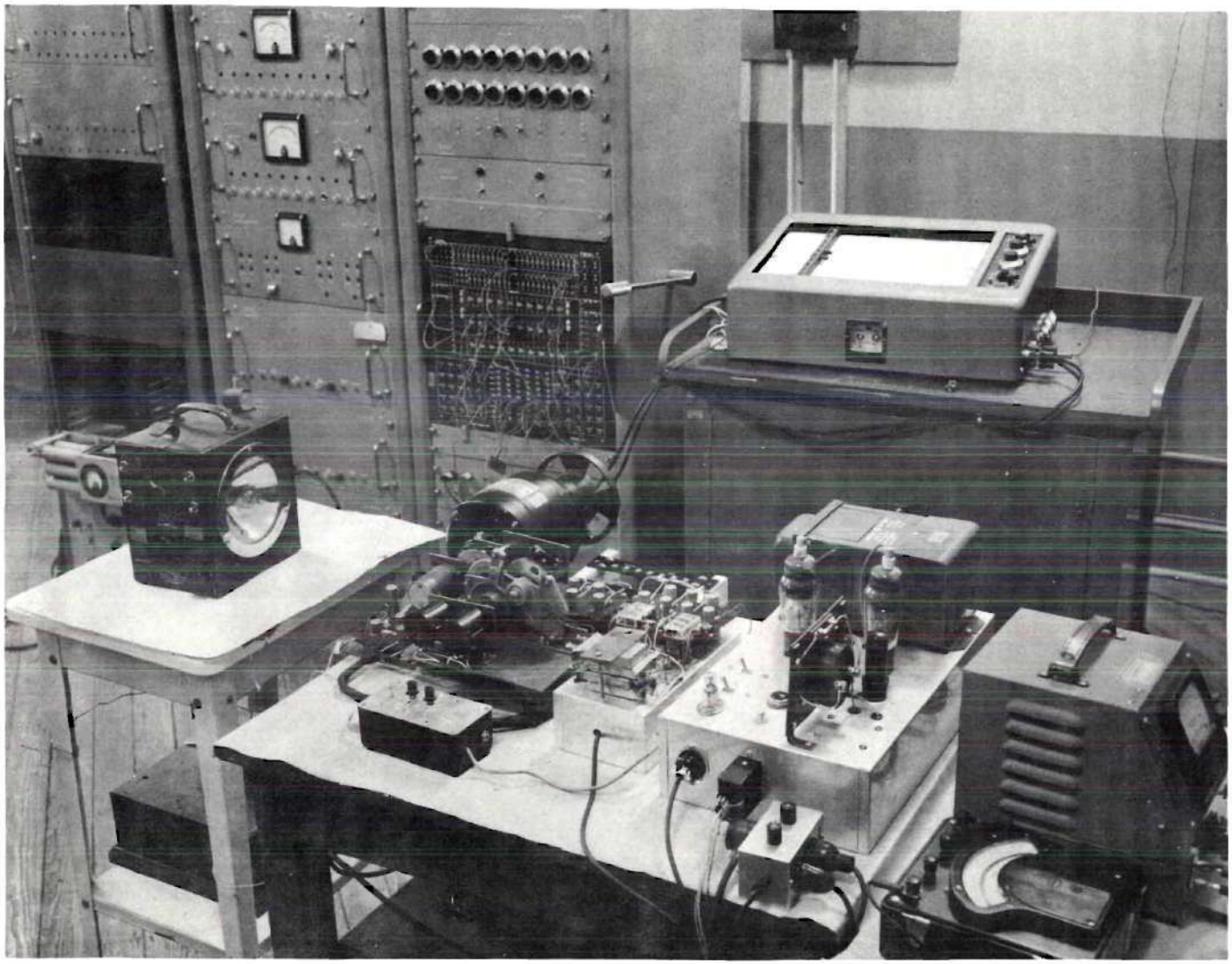

Figure 15. View of the Laboratory Model.

or

$$v_s = \frac{E_p}{\frac{r}{GK_T} + K_b} . \tag{54}$$

When the approximate time constant and saturation velocity are determined, the gear ratio is chosen to effect the best display of error within the ten-turn capability of the output potentiometer.

The gear ratio of the laboratory model (16.5) enables the output shaft to travel at the saturation velocity (8.95 rad./sec.) through an angle

$$c = q\, v_s \tag{55}$$

during time $t = q$ ($q = 2.49$). Expressed numerically, (55) becomes

$$c = 3.5 \text{ rev.}$$

This angle corresponds to a non-dimensional error displacement given by

$$|x| = \left|\frac{c}{qv_s}\right| = 1 . \tag{56}$$

The gear ratio 16.5 was then chosen so that this error magnitude on the non-dimensionalized phase plane corresponded to 3.5 revolutions of the output potentiometer. Since the output potentiometer has a useful range of 8 revolutions (2 are reserved as safety zones), a non-dimensional error range of

$$x = \frac{8 \text{ rev.}}{3.5 \text{ rev.}} = 2.28 \tag{57}$$

could be displayed. This range was adequate to obtain all of the trajectories used in this thesis.

This gear ratio was obtained by the use of an idler shaft between the motor and output shafts. The gear mechanism is shown in Fig. 29 of Appendix A. In order to protect the potentiometer, motor reversing limit switches were also included in the gear assembly. These were incorporated by the use of a 837/40 speed reduction from the output shaft to the cam shaft. The limit switches were placed 138° apart at the cam corresponding to an eight-revolution excursion of the output shaft.

Motor circuits.--The motor and associated components of the mechanical assembly are shown schematically in Fig. 32 of Appendix A. The 200-volt potential at terminal "a" energizes the motor field and armature. Armature current flows from terminal "a" through the series field and a 333-ohm resistor to the contacts of a reversing relay. The two reversing relays are wired so that one of the 333-ohm resistors is in series with the armature whenever power is supplied to the armature. The value 333 was determined by the choice of G explained earlier. Power is supplied to the armature from the power supply when one relay is energized and the other is de-energized. The applied voltage (E_p) is reversed when the status of the two relays is reversed.

The relays are energized when the 24-volt potential appearing at terminals "j" and "k" is applied to terminals "l" or "o" for the upper relay and terminals "u" or "p" for the lower relay. The 24 volts are applied to these points either by the computer operational relays (Fig. 30 of Appendix A, terminals "e" and "j" or "m" and "k") or by depression of the lever switch in the manual control unit (Fig. 31-a of Appendix A,

terminal "o" or "p"). The relays are energized through the two limit switches. The actuation of either limit switch causes the status of the relays to reverse, which reverses the motor. Spark suppression circuits are shown across each relay contact. The tachometer output contains a ripple suppression capacitor.

The power supply, illustrated schematically in Fig. 33 of Appendix A, was designed specifically for the system. Thyratron tubes are diode-connected in the high-voltage rectifier. Two separate selenium rectifier units are used to supply 24 volts to the relays and tachometer field. The use of separate rectifiers minimized the voltage variations of the tachometer field.

Fig. 31-b of Appendix A is the schematic diagram of the manual switch unit which gives the operator control of the motor and simultaneously opens the error loop when either the "forward" or "reverse" lever is depressed. When the loop is closed, the relay energizing potential (24 volts) appears on terminal "n". When the loop is open, this voltage appears on terminals "o" or "p", but not both, according to which lever switch is actuated.

Computer circuits.--The analog computer circuits used in the laboratory model are shown in Figs. 30 and 31-a of Appendix A. Input terminals "g" and "h" are connected to the input and output potentiometer arms. In the first stage these signals are added and amplified by 1.5; the resulting amplified sum represents the system error, which is one input to the second adder and also the x input to the x-y recorder. The other input to the second adder is the output of the function generator. The

input to the function generator is the derivative signal supplied by the tachometer connected to terminal "i". The derivative signal is amplified by two cascade stages with a total gain of 25. The output of the first amplifier represents the error derivative and is the y input to the x-y recorder.

The output of the second adder represents the left-hand side of (33), the sum of the error and the modified derivative signals. The output of the second adder drives the two relay channels. Each channel consists of a unity-gain amplifier and a high-gain amplifier. The purpose of the high-gain amplifier is to translate a change of polarity at the output of the second adder to a large voltage sufficient to energize the operational relay. Each channel is provided with a variable bias to adjust the hysteresis zone of the relay to give the proper inactive zone configuration as discussed in Chapter III. Adjustment of the biases in both channels establishes the values "a" and "b" associated with the inactive zone in Fig. 11. The operational relays are polarized oppositely to respond to either positive or negative signals from the second adder. However, during the transition through the inactive zone both relays are activated.

The upper contacts on the operational relays control the coil circuit of the motor-reversing relays discussed previously. The lower contacts are used for plotting the relay action on the "Sanborn" dual-channel recorder. The associated circuits are shown in Fig. 31-a of Appendix A. The three 100-k resistors constitute a voltage divider. The voltage output is approximately 18.5 volts if neither or both of the contact sets

"u"-"v" and "s"-"t" are shorted. However, if only one of the operational relays is energized, only one of the 100-k resistors is shorted. The output to the recorder will accordingly be more or less than 18.5 volts depending upon which resistor in the chain is removed. This circuit was the means of obtaining the time response data in Fig. 26.

Experimental determination of the switch boundary.--The output of the function generator has been defined by (32) and the switch locus by (33). Instead of realizing $g(x)$ from its analytical expression, it is convenient to determine $g(x)$ experimentally using a method suggested by Hopkin (19). This procedure is illustrated in Fig. 16. The transformation of the phase plane to the $g(x') - x'$ plane is performed graphically.

The decelerating trajectory is first obtained on the x-y recorder. Then the transformation is made through the desired switch plane, to the $g(x') - x'$ plane, point by point. For the equal voltage scales given, this amounts to rotating the phase-plane decelerating trajectory 90° clockwise and relabeling the ordinate, $g(x')$, and the abscissa, x'.

Once the $g(x') - x'$ curve is obtained, the voltages V_a and V_b can be read directly from the curve for a number of points. Then, with the function generator circuits isolated as indicated in Fig. 16, for each point, the voltage V_a at the input should produce the corresponding voltage V_b at the output. By this process the slopes of the 20 approximating segments are adjusted. The output of the second adder with the function generator reconnected now represents the locus $x + g(x)$.

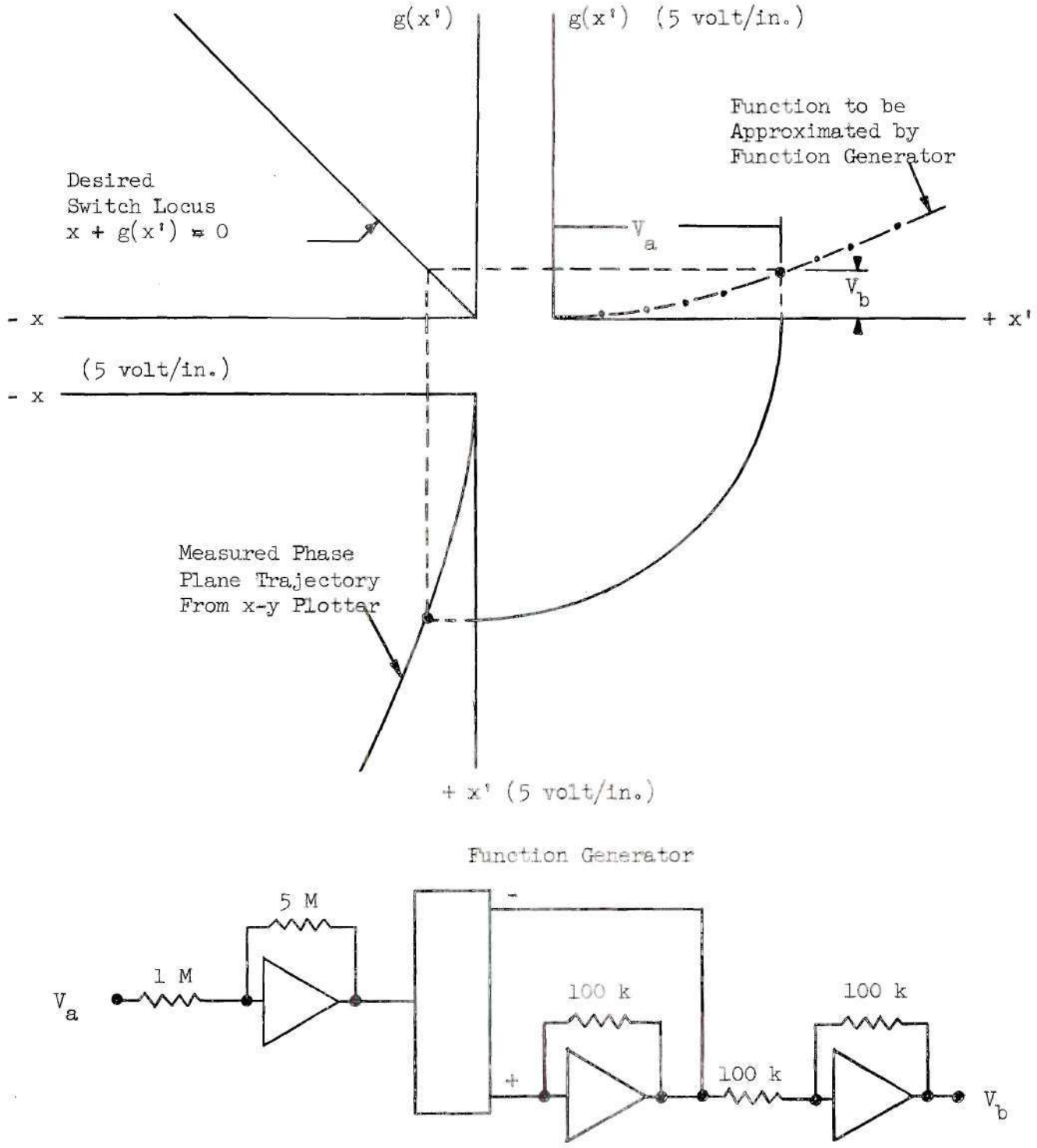

Fig. 16 Determination of the Switch Boundary Experimentally

The final step in the realization process is to adjust the bias values in the relay drive circuits so that the switch boundary conforms to the configuration of Fig. 11. After this adjustment, the system is operative.

CHAPTER V

EVALUATION OF THE SYSTEM

Determination of constants.--After the laboratory model was found to be operative, it was subjected to the various response tests described later in this chapter. As a means of evaluating these data, these results are compared with the analytical results described in Chapter III. In order to make a direct comparison between the two forms, the constants involved in the equations of Chapter III had to be evaluated for the system under test. The motor constants were determined before the assembly of the equipment. The other constants were determined after all of the response data were obtained. All constants are computed in Appendix D.

For convenience in computation, all of the motor data have been referred to the output shaft. Constants K_b and K_T are calculated from the slopes of the straight line relations in Figs. 34 and 35 of Appendix B. In similar manner the tachometer speed-voltage transfer constant K_d is determined from Fig. 36. The viscous coefficient, γ, and the dry-friction torque, T_F, were found by allowing the complete system to run at several saturation velocities. The armature current was recorded for each value of saturation velocity, and the corresponding torque was calculated and is shown graphically in Fig. 37 of Appendix B. The slope of the resulting line gives the viscous coefficient γ, while the intercept at zero speed is the constant dry-friction torque, T_F.

The next constant to be found was the total viscous coefficient f. The defining relation (49) indicates that the conductance G must be found prior to f. The conductance G may be computed from

$$G = \frac{1}{R} = \frac{1}{R_a + R_d + R_p + R_s} \quad . \tag{58}$$

The test data for determining each of these resistances are given in Fig. 38 and Tables 1 and 2 of Appendix B.

The total inertia and time constant of the system remained to be found. This is obtained from the solution of

$$Jc'' + fc' = T \tag{59}$$

for the initial conditions,

$$\begin{aligned} c' &= 0 \\ c &= 0 \\ t &= 0 \ . \end{aligned} \tag{60}$$

After substitution for J, f, and T, (59) becomes

$$qc'' + c' = v_s \tag{61}$$

which may be integrated to obtain

$$c' = v_s(1 - e^{-\frac{t}{q}}) \tag{62}$$

or

$$e^{-\frac{t}{q}} = (1 - \frac{c'}{v_s}) \ .$$

Then,

$$q = \frac{-t}{\ln\left(1 - \frac{c'}{v_s}\right)} \tag{63}$$

and J is computed from

$$J = f\ q\ . \tag{64}$$

These relations allow the determination of q and J by an acceleration test of the complete system. The test is shown graphically in Fig. 39. The acceleration interval is expressed analytically by (62). To insure that the test velocity followed the exponential relation (62), the normalized velocity was replotted on a logarithmic scale (Fig. 40 of Appendix B). The time constant was then computed as the inverse slope of the linear portion of the curve or from relation (63).

Calculated response.--All of the calculated phase plane trajectories shown in the figures in this chapter were drawn using the open circuit template of Fig. 9. The data relating to this curve are given in Tables 3 and 4. In cases where the time response of the calculated phase plane trajectory was to be compared with the observed time response, (25) was utilized to compute time. The coordinates of the calculated trajectory were substituted in this equation, and the corresponding time was determined. This equation is the basis of Tables 7 and 9. In all comparisons the observed responses were non-dimensionalized, so that the trajectories are plotted on the non-dimensional plane, and the time responses are plotted against dimensionless time, p. Whenever comparisons

are made, the transformation from observed data to non-dimensional data is shown in the tables. Sample computations appear in Appendix D.

Discussion of results.--The observed open loop trajectory is plotted in Fig. 17. The similarity to the analytical prediction of Fig. 9 is at once apparent. With the system's error loop opened, the switch boundary was determined and was plotted in Fig. 18, where the first and final approximations are shown.

The first approximation was obtained by the procedure outlined previously (Chapter IV). The use of this switch boundary resulted in considerable overshoot when large initial velocity corrections occurred. This overshoot can be attributed, not only to the original misalignment of the curve, but to the previously discounted finite relay-transition interval. For a given interval a greater horizontal distance is traveled at high velocities than at low velocities. At high velocities, the final trajectory is displaced farther from the boundary through the origin than at low velocities. The resulting e-axis intercept is correspondingly displaced outside of the inactive zone with the accompanying overshoot. This difficulty is remedied by advancing the switch boundary in the plane as indicated by the final boundary of Fig. 18.

This switch boundary was used in the final predictor system. The boundary effected the desired system performance for any input magnitude. The resulting phase plane trajectories for various magnitudes of initial displacement are shown in Fig. 19. Regardless of the magnitude of the initial error, one torque reversal takes place and the system comes to rest at a predetermined steady-state error (e intercept) with no overshoot.

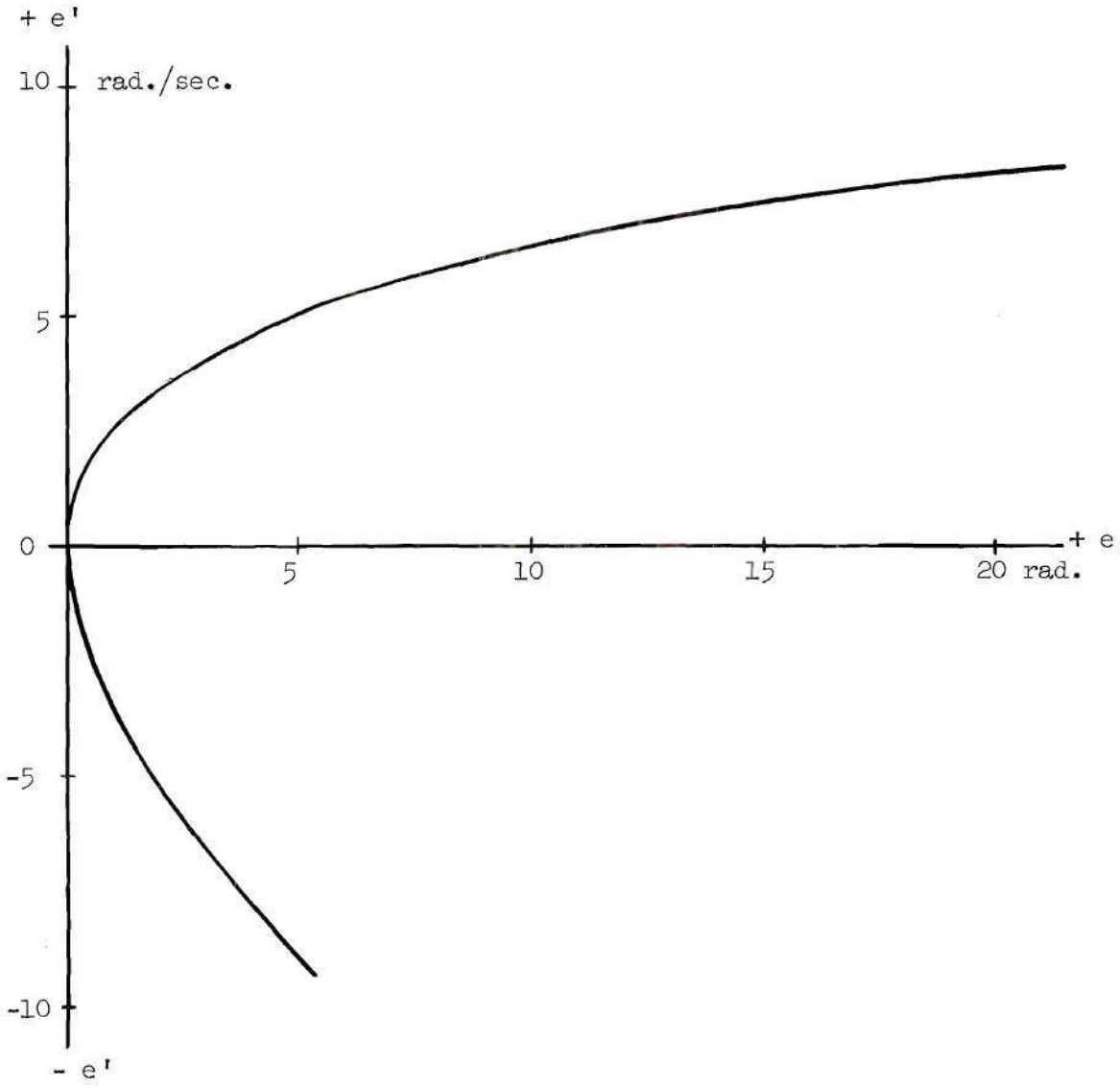

Fig. 17 Observed Open Loop Trajectory

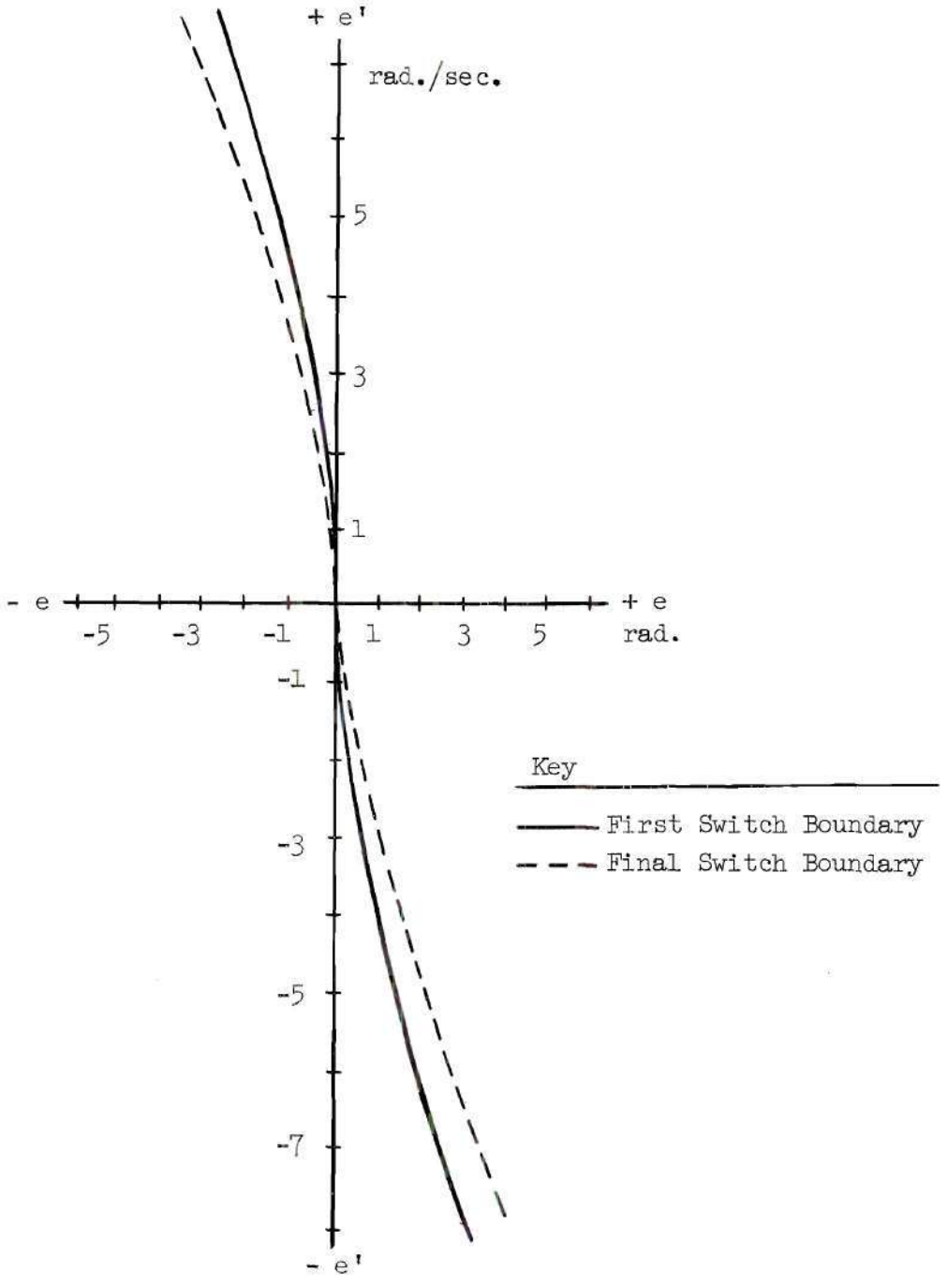

Fig. 18 Observed Switch Boundaries

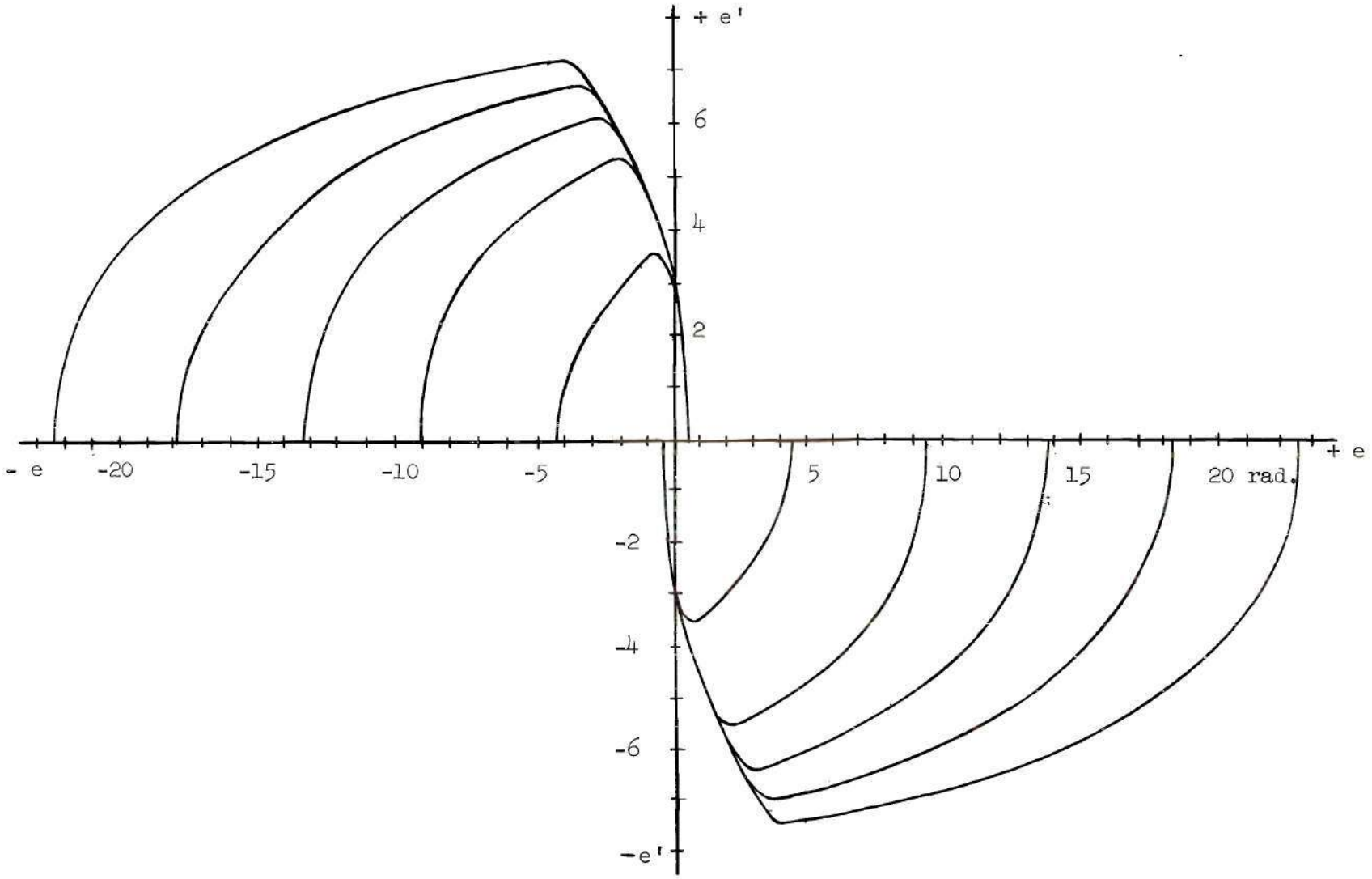

Fig. 19 Trajectories of the Predictor System for Several Displacement Inputs

Comparison of observed and calculated response.--One of the basic objectives of this thesis is to compare a physical predictor system with its analytical counterpart and thereby ascertain what deviations from the theoretical promise, if any, exist. In this section the response of the laboratory model and the theoretical model derived in Chapter III are compared. The open loop trajectories are analyzed first, and then the response to a displacement input, and finally the response to a displacement input plus initial velocity.

The comparisons of open loop trajectories are given in Fig. 20 and Tables 3, 4, 5, and 6. The calculated trajectory was plotted by template, while the observed trajectory was non-dimensionalized for comparison. The lack of confluency observed in all of these comparisons, which amounts to approximately ten per cent, resulted from a corresponding change in motor field current between the performance tests and the evaluation of constants. The changed current caused the system torque to change with the resulting apparent "faster" response of the observed system. This discrepancy brings to light one of the limitations of predictor systems to be discussed later. It does not affect the consistency of these comparisons. This is easily proven by multiplying the measured torque constant by another constant and substituting into the analytical expressions. The resulting graphs will correlate very closely with the observed responses. This proof was not made in this thesis since it would, in effect, be deemphasizing the effect of parameter variance on predictor performance.

The comparison of time response of the theoretical and the laboratory systems appears in Fig. 21. A displacement input of 12.6 radians was applied to both systems.

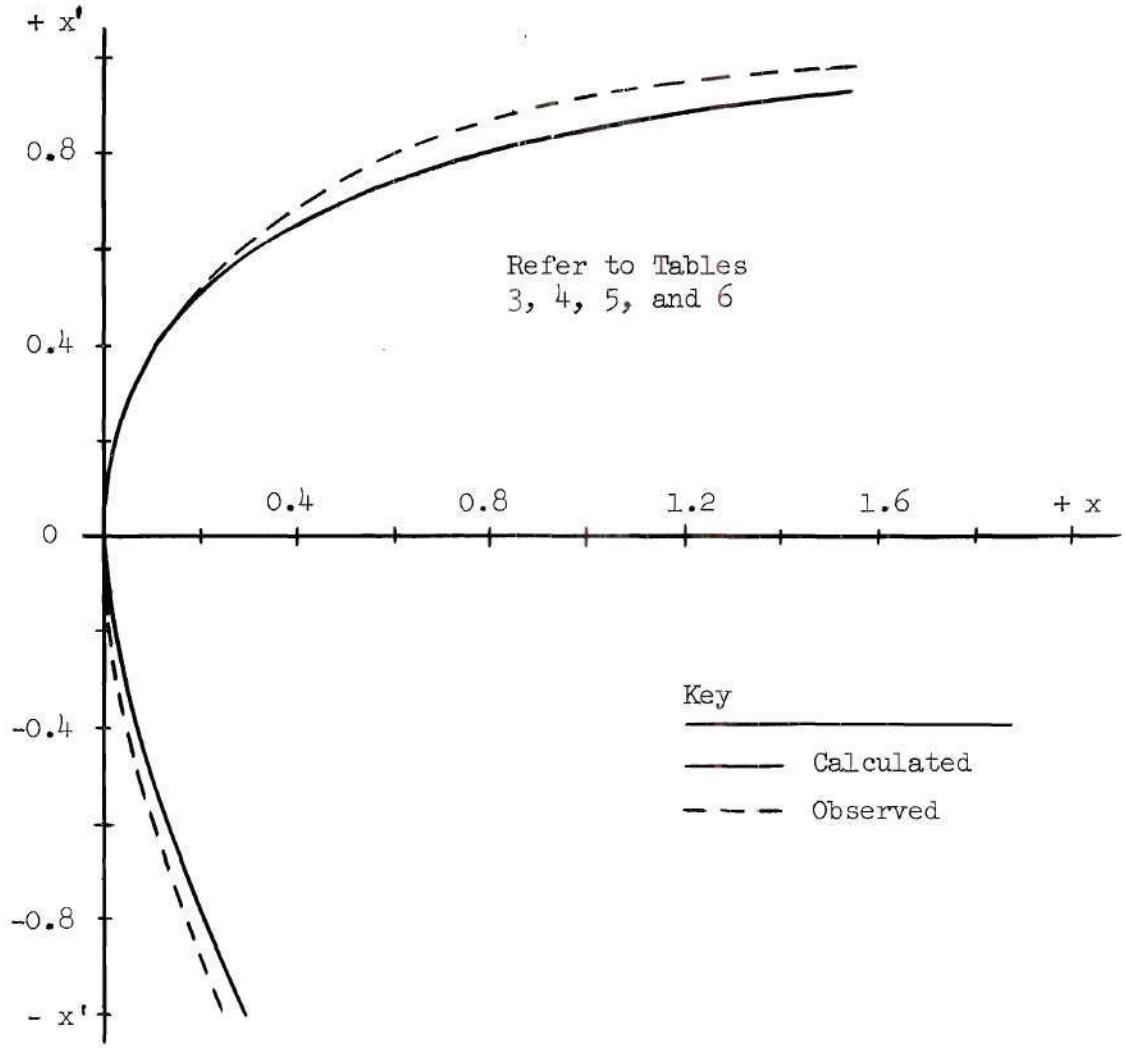

Fig. 20 Non-dimensional Open Loop Trajectories

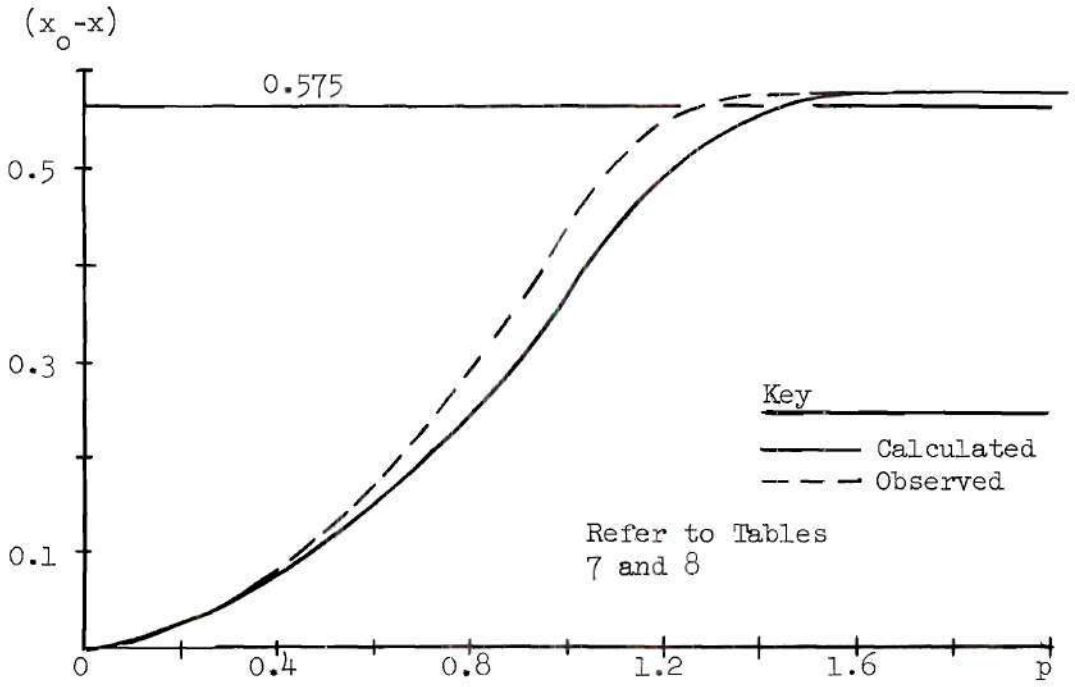

(a) No Initial Velocity

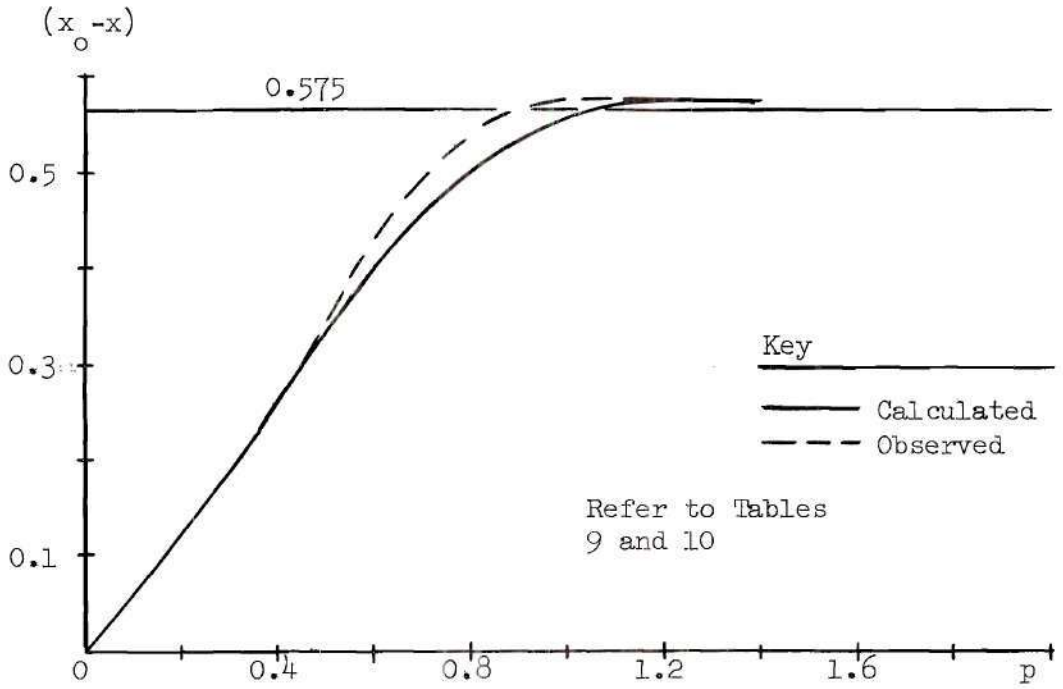

(b) With Initial Velocity

Fig. 21 Predictor Non-dimensional Time Response

The upper graph describes the case with no initial velocity; the lower graph, an initial velocity of 4.87 rad./sec. The computation of time for the calculated curves appears in Tables 7 and 9. Tables 8 and 10 illustrate the manner that the observed data are non-dimensionalized. The corresponding phase plane trajectories for the responses illustrated in Fig. 21 are given in Figs. 22 and 23 for the same initial conditions.

Comparison with an uncompensated system.--The observed predictor responses of Figs. 21, 22, and 23 are replotted on dimensional scales in Figs. 26 and 27 so that they may be compared with the uncompensated equivalent system. The uncompensated equivalent system responses are plotted in Figs. 24 and 25. This system has the same dynamic characteristics as the predictor system. It is devised from the predictor system by disconnecting the function generator signal at the input to the second adder shown in Fig. 30 of Appendix B.

The switching in this case depends on the polarity of the error, and the switch boundary is the vertical axis in the phase plane. The width of the inactive zone remains the same as the inactive zone in the predictor system. Only the switch boundary is affected by the conversion to the uncompensated system. The underdamped responses of Figs. 24 and 25 and the accompanying long settling times may be contrasted with the predictor performance of Figs. 26 and 27. Fig. 28 provides a direct comparison of the settling times of the two systems. It is also of interest to note that with the same input conditions the predictor torque changed polarity once, while the uncompensated system reversed its torque six times for the displacement input and seven times for the displacement input plus initial velocity.

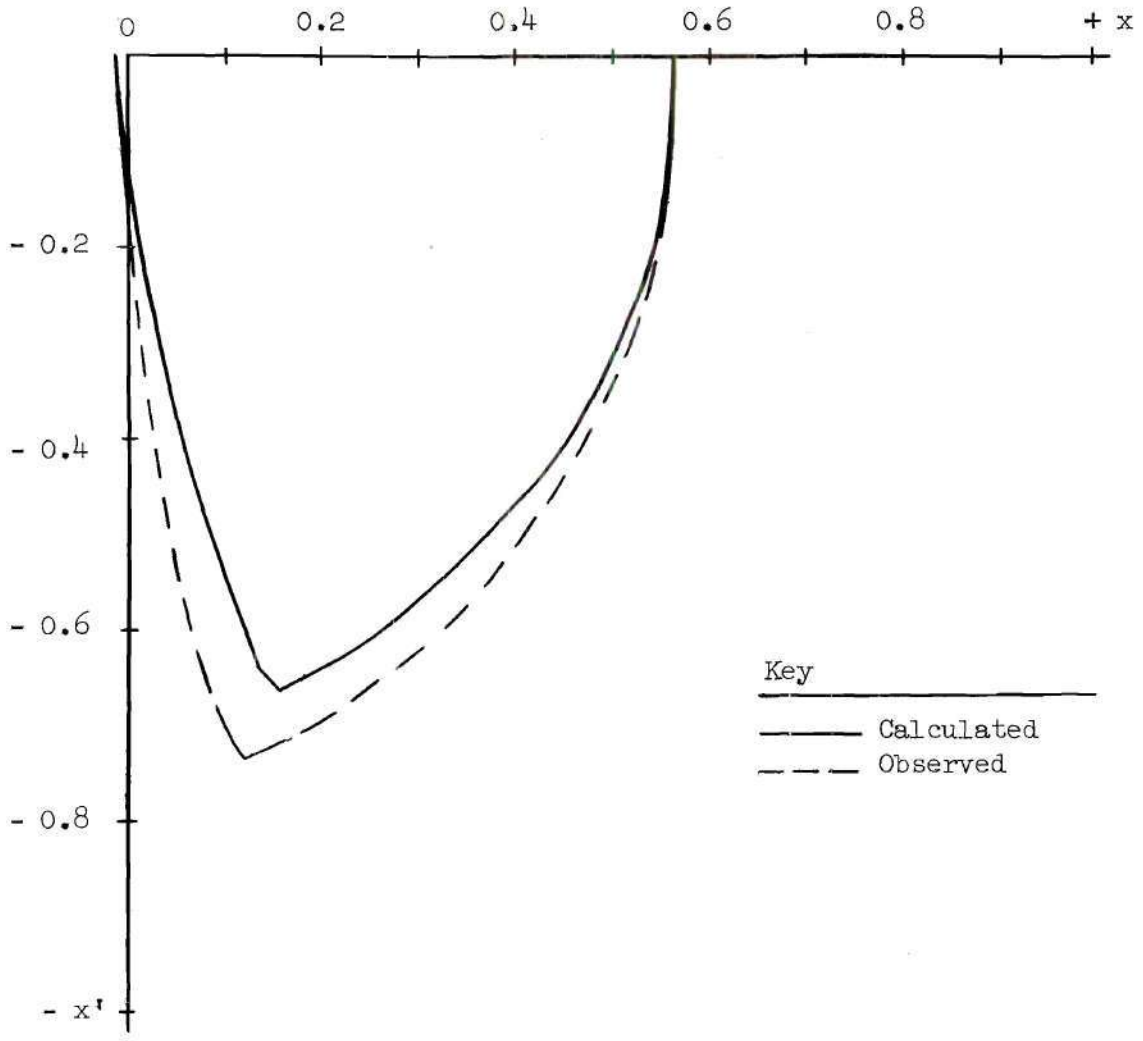

Fig. 22 Predictor Non-dimensional Trajectories for Displacement Input

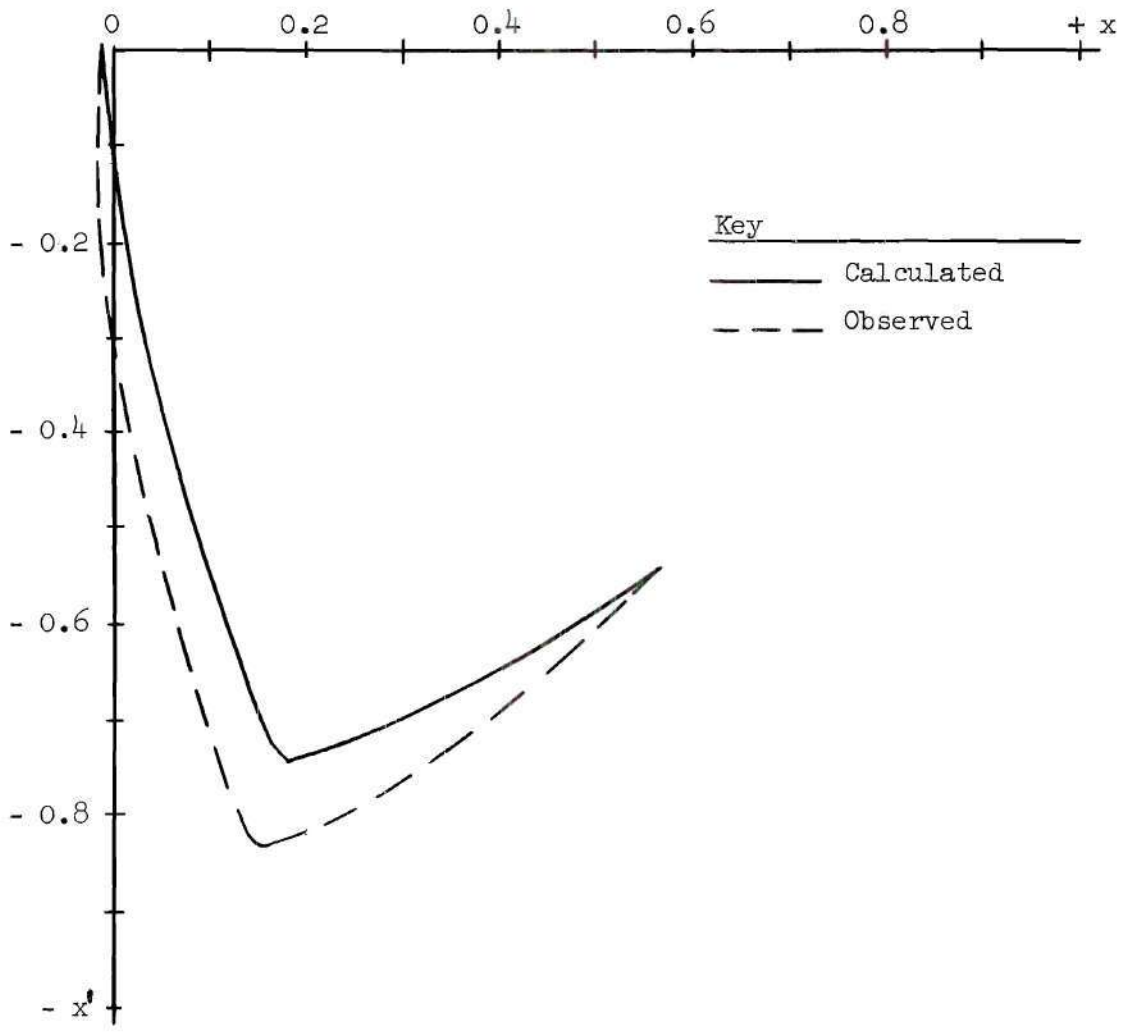

Fig. 23 Predictor Non-dimensional Trajectories for Displacement Input and Initial Velocity

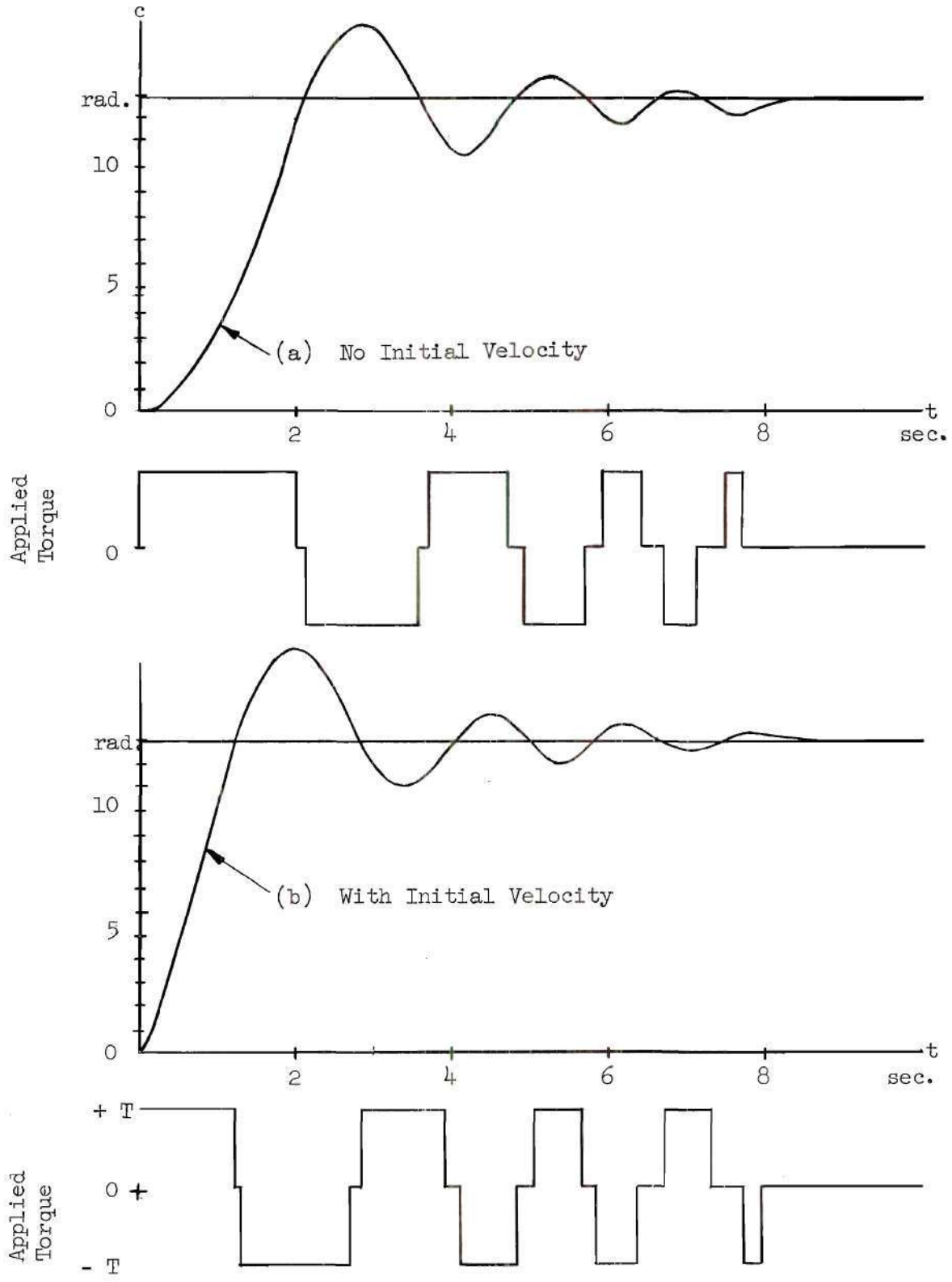

Fig. 24 Uncompensated Equivalent System Time Response

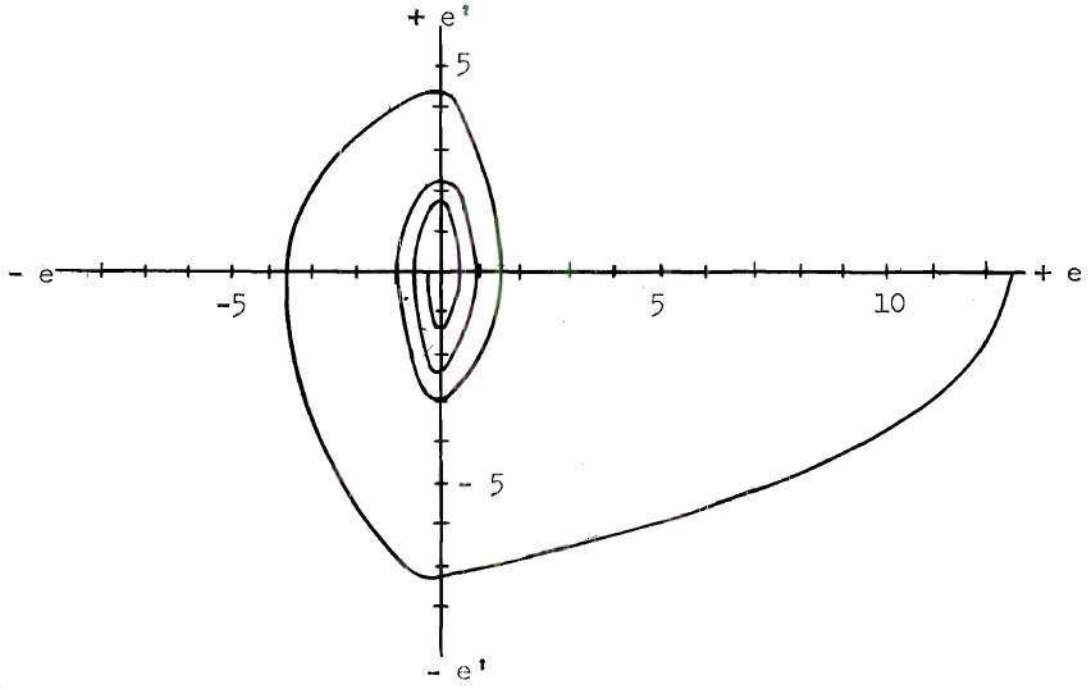

(a) No Initial Velocity

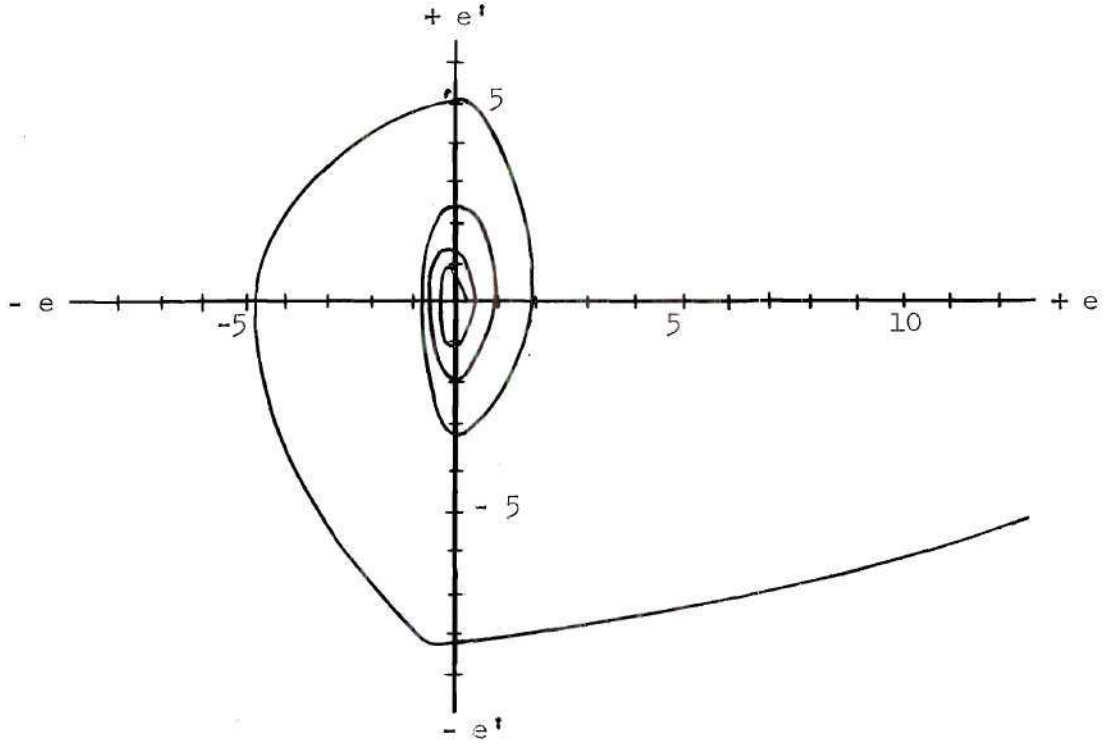

(b) With Initial Velocity

Fig. 25 Uncompensated Equivalent System Trajectories

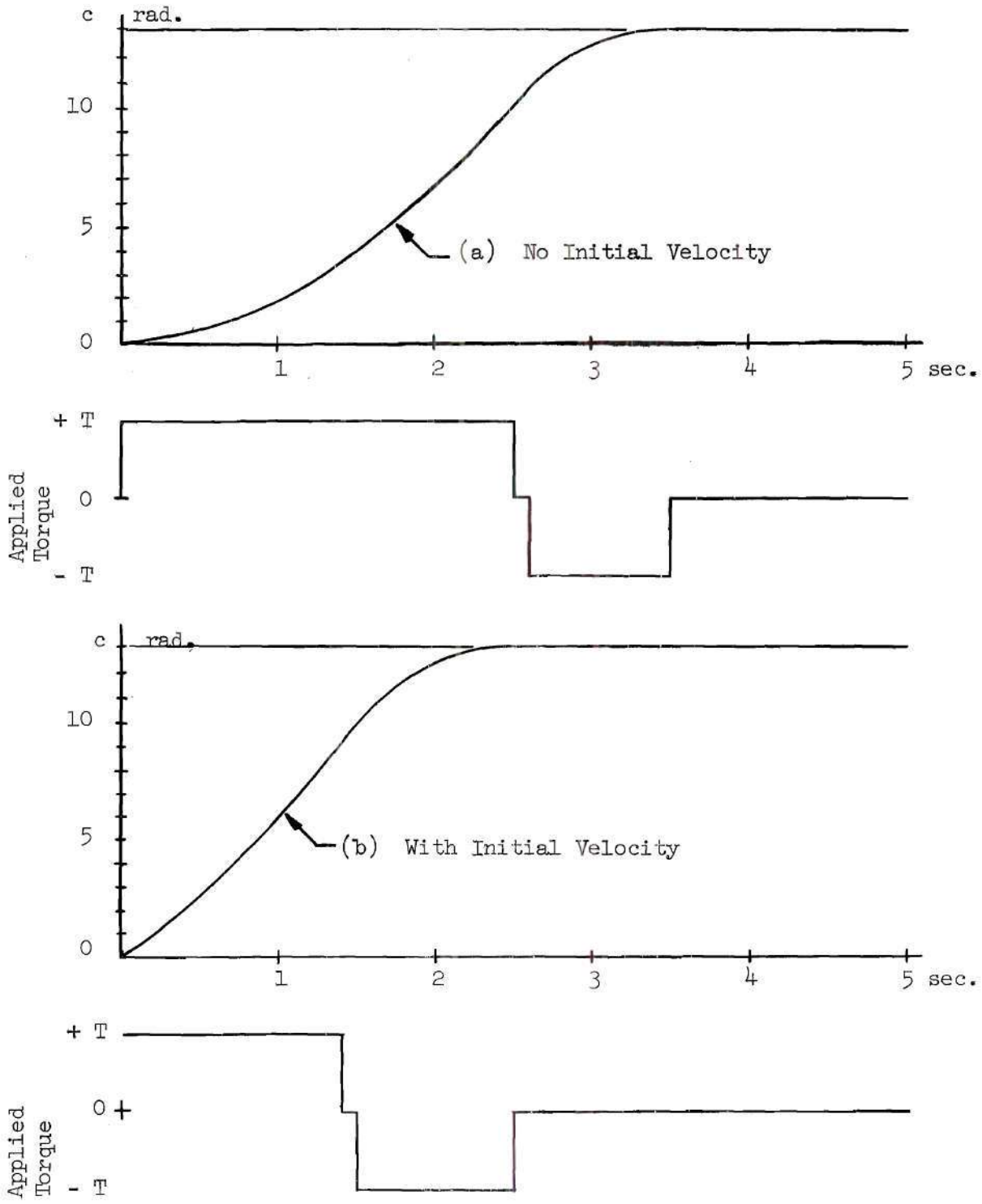

Fig. 26 Predictor Time Response

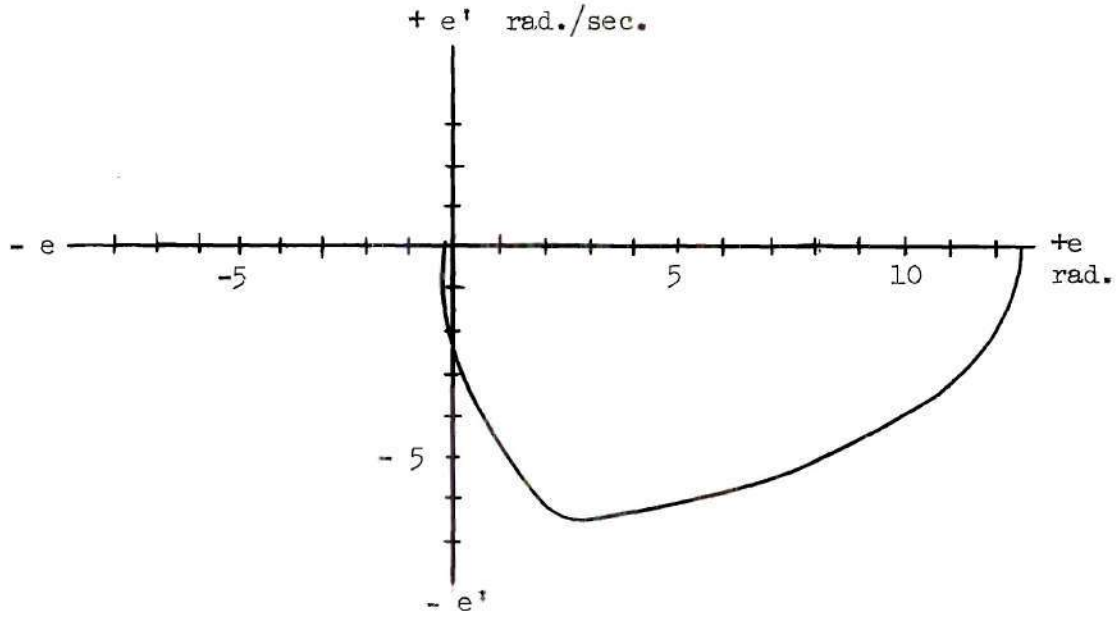

(a) No Initial Velocity

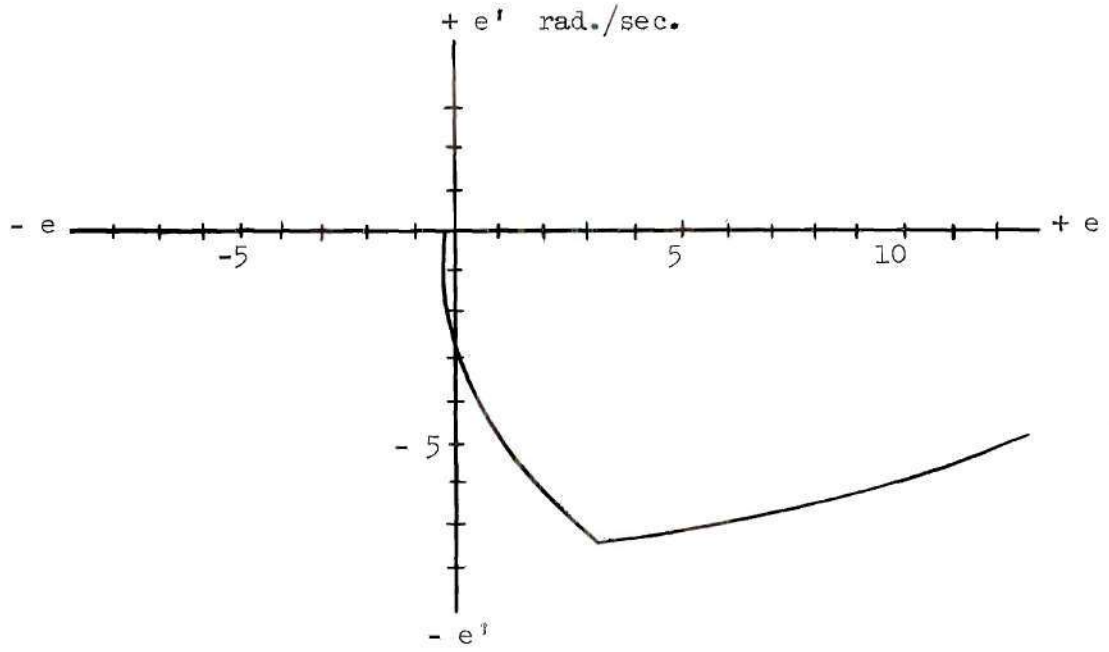

(b) With Initial Velocity

Fig. 27 Predictor System Trajectories

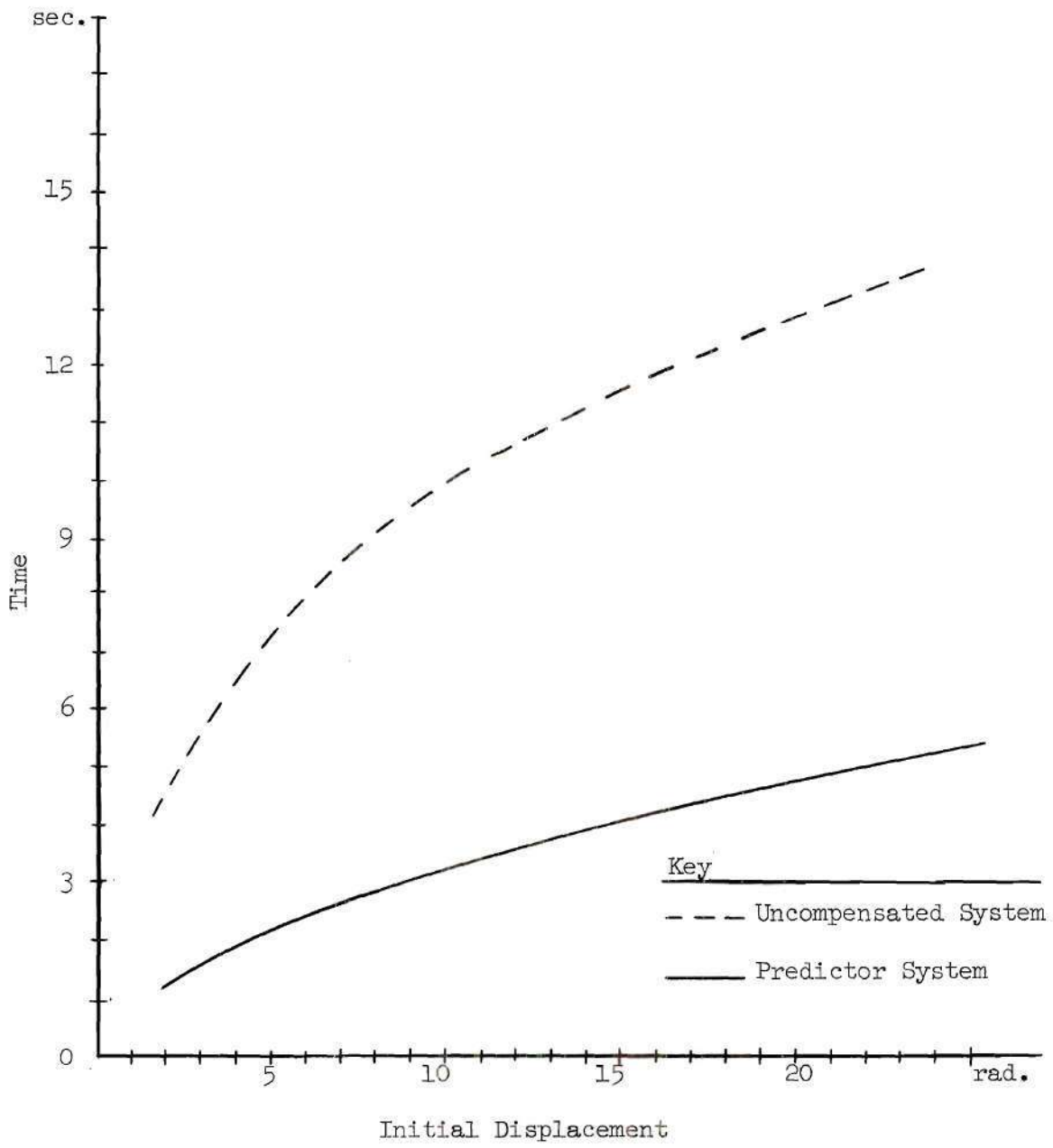

Fig. 28 Time to Reach 0.25 Radians Error

The stability of the predictor system, like that of the uncompensated system near the origin of the phase plane, depends upon the alignment of the hysteresis zones of the relays and upon the width of the inactive zone. The tendency to oscillate near the origin was not noticeably decreased or increased by the predictor controller.

Since the switch boundary is derived from the dynamic characteristics of the system, any change in the dynamic parameters will affect the switch boundary. A slight change in the field current in the motor, for instance, changing the torque, causes the switching to become erratic because of the misplacement of the switch boundary. This sensitivity suggests that the predictor system is very sensitive to its dynamic environment.

CHAPTER VI

CONCLUSIONS AND RECOMMENDATIONS

Conclusions.--This thesis has investigated a new method of optimizing the performance of a second-order contactor servomechanism. The differential equations of motion of the servomechanism, which included the effects of inertia and viscous damping, were solved and transformed to the phase plane. By the use of the phase plane, a relation between the error and the error time derivative was found which exists when optimum switching occurs. This relation describes the switch boundary in the phase plane where the corrective torque must be reversed if optimum response is to result. Optimum response is characterized by the reduction of the error and error derivative to minimum and zero respectively.

A laboratory model which incorporates this method of switch control was constructed, and the response to displacement inputs was observed. This response was compared with the calculated response and with that of an equivalent uncompensated system.

The laboratory model displayed optimum response to displacement inputs ranging from 4 to 24 radians magnitude. Optimum response was still obtained when the displacement occurred while the output shaft was in motion.

The nonlinear function of the error derivative in the switch controller for the laboratory model is expressed analytically as

$$g(x') = [\,|x'| - \ln(1 + |x'|)]\,[\mathrm{sgn}(x')] \quad . \qquad (32)$$

An approximation of this function was determined experimentally from the open loop trajectories and realized by a biased-diode function generator.

Within a ten per cent margin the calculated response agreed with the observed responses. This ten per cent deviation is attributed to a power-supply voltage variation which occurred during the evaluation. The equations and graphical techniques developed here should prove useful in the design of practical predictor systems.

These conclusions apply to a second order contactor system used to position an inertial load with viscous damping. The controller described can be used only where the dynamic parameters J, T, and f are invariant. In addition, the system is designed specifically for the correction of displacement errors.

Recommendations.--The limitations of the predictor controller described in this thesis have been stated in the Conclusions. An analysis is needed for the design of these systems which does not restrict the input to be a step function (or ramp function). Simplified design procedures for third and higher order systems would be helpful. An analysis which would allow the dynamic parameters to be functions of time would increase the acceptability of predictor systems.

Several improvements could be made on the laboratory model. A regulated power supply would eliminate the torque variations. The existing systems could also be converted to a quasi-linear (dual-mode) system, which would conserve power consumption by proportional correction of small errors.

APPENDIX A

DIAGRAMS

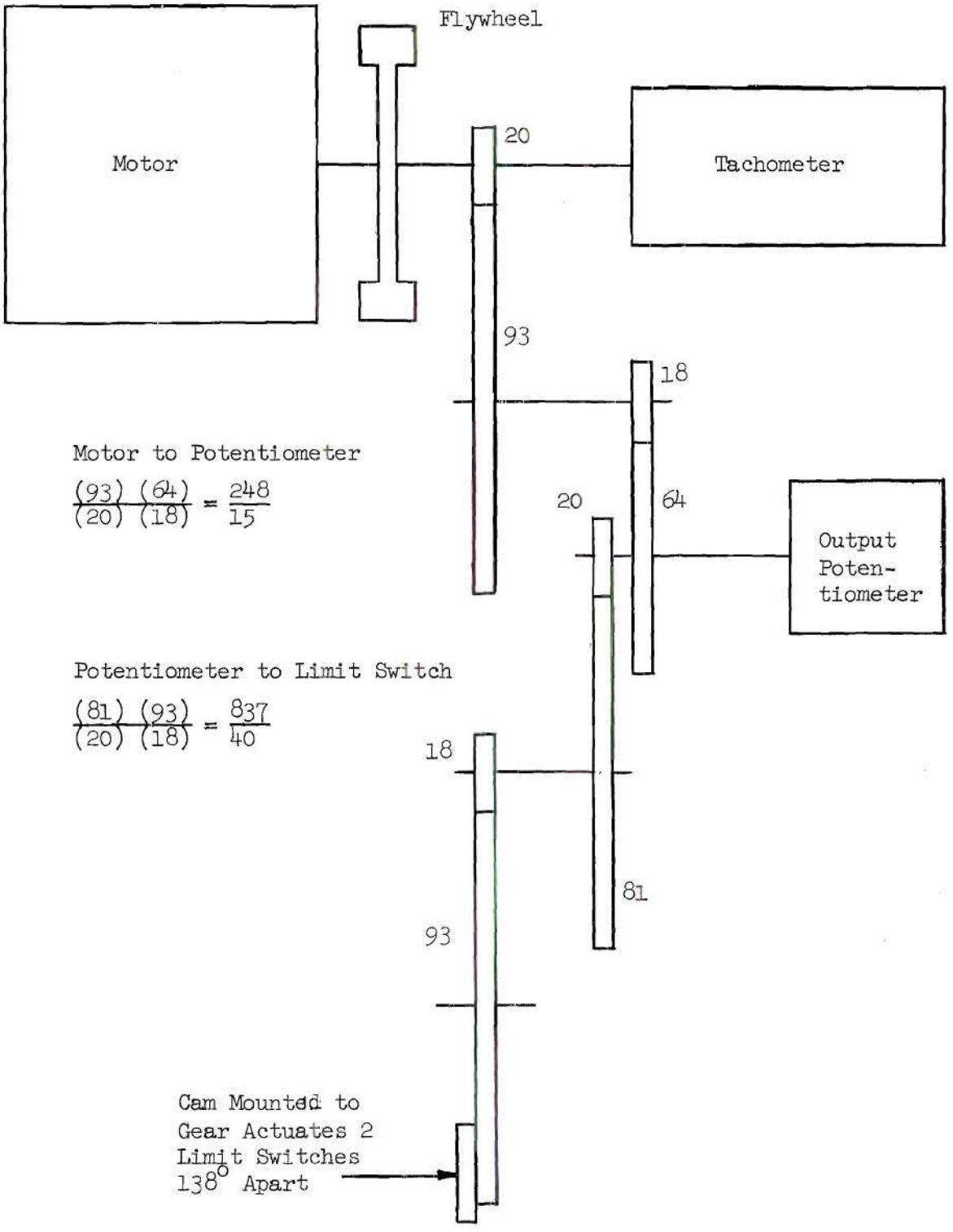

Fig. 29 Gearing Diagram

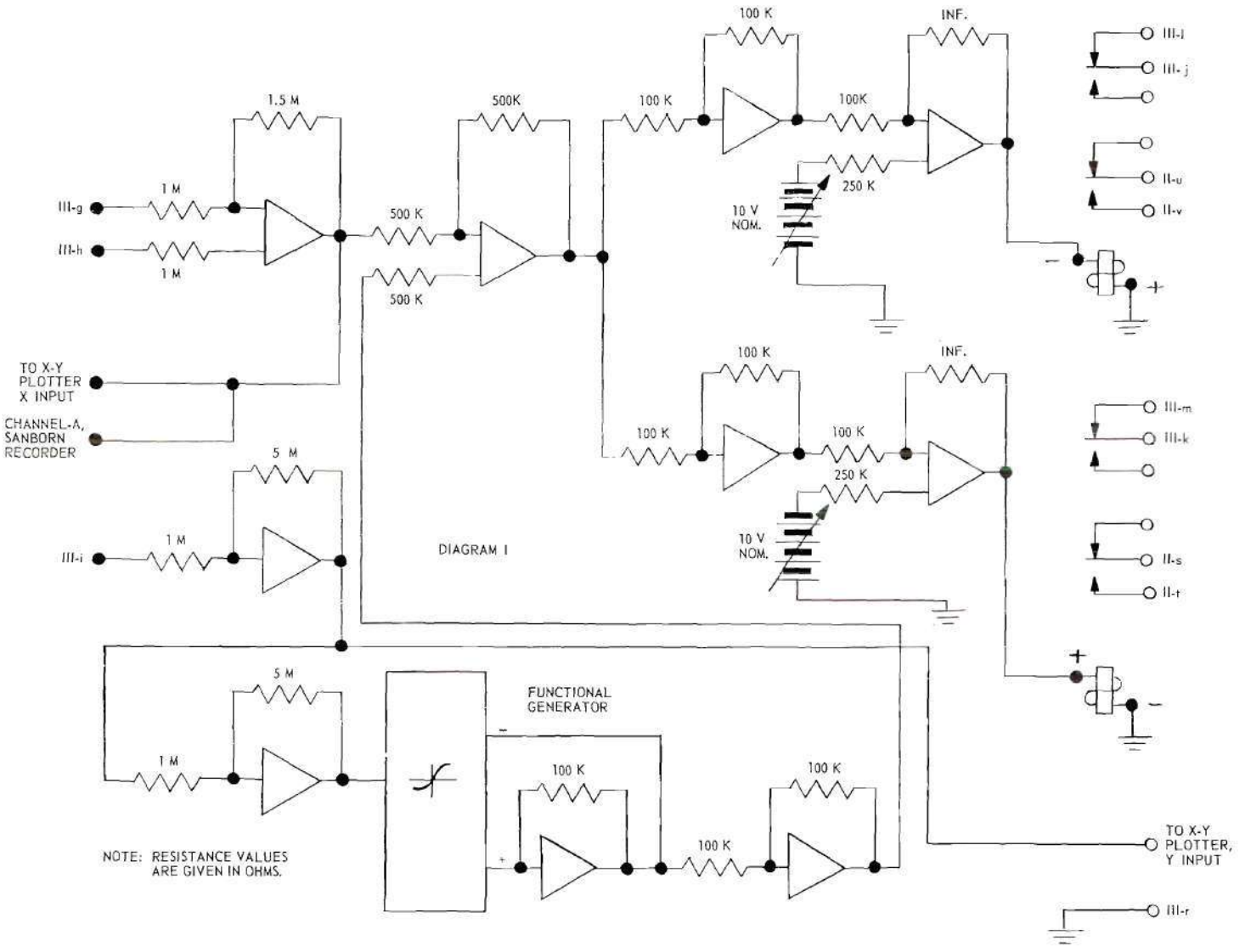

Figure 30. Analog Computer Circuits.

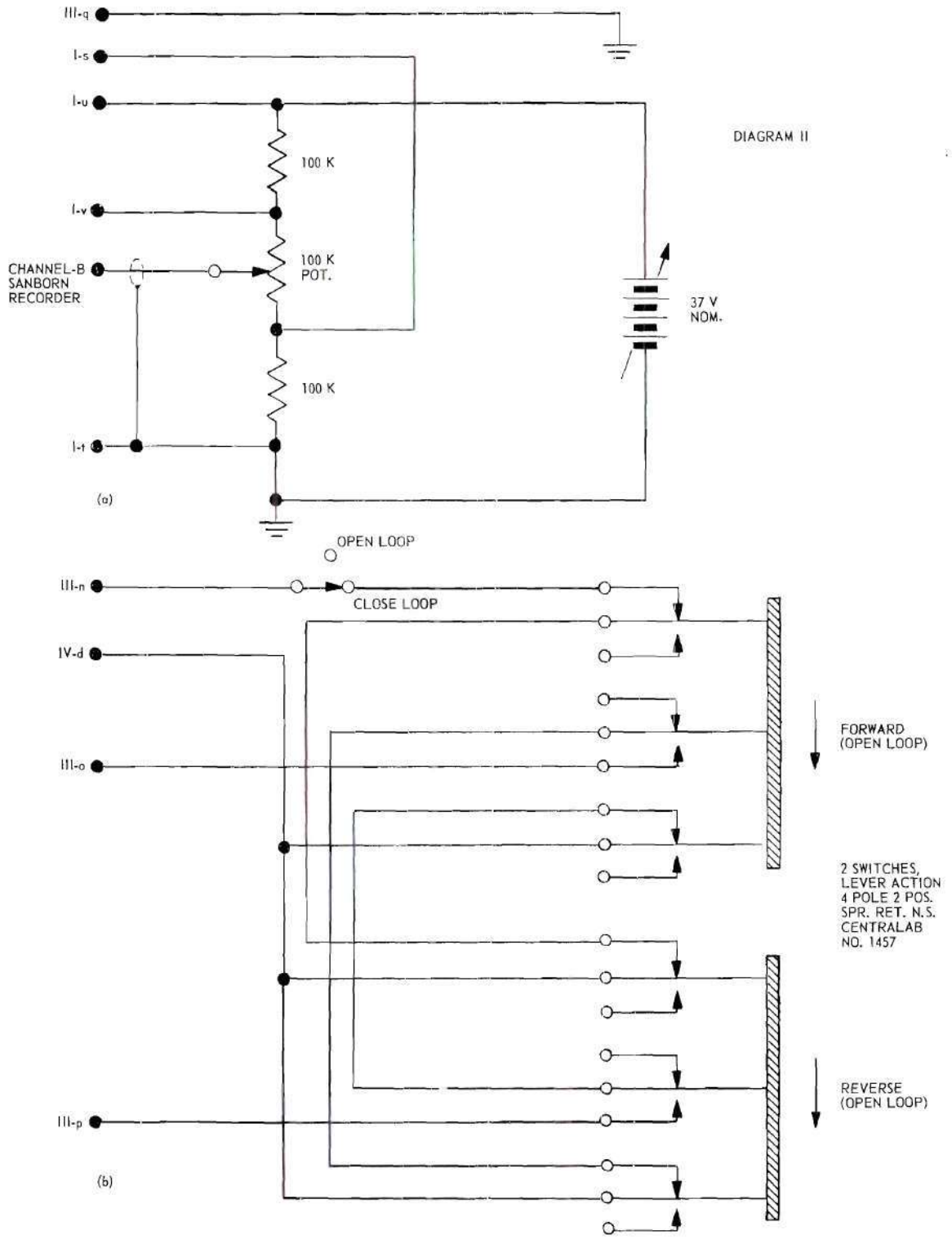

Figure 31. Relay Plotting Signal Source and Manual Switch Unit Circuits.

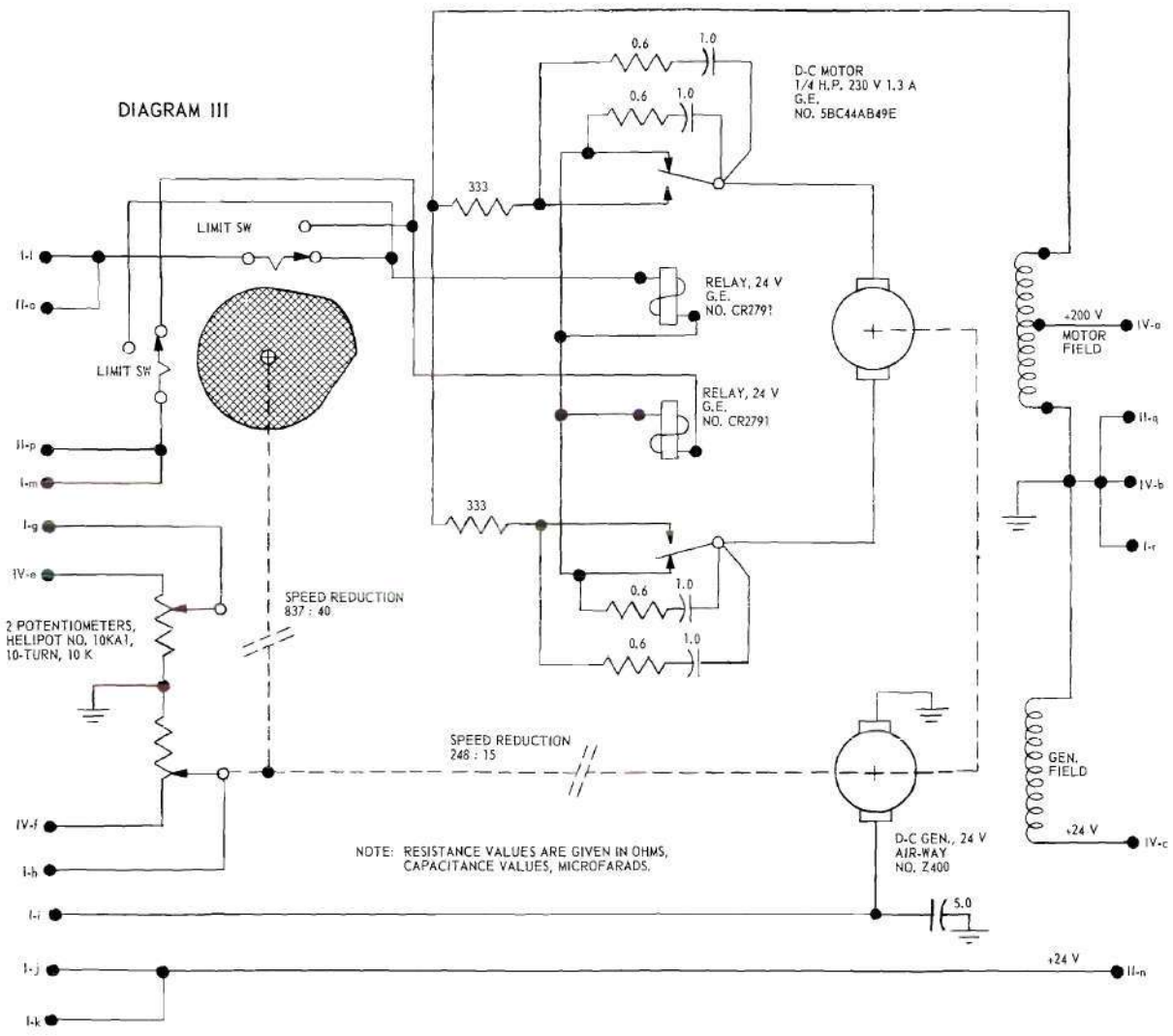

Figure 32. Motor Circuits.

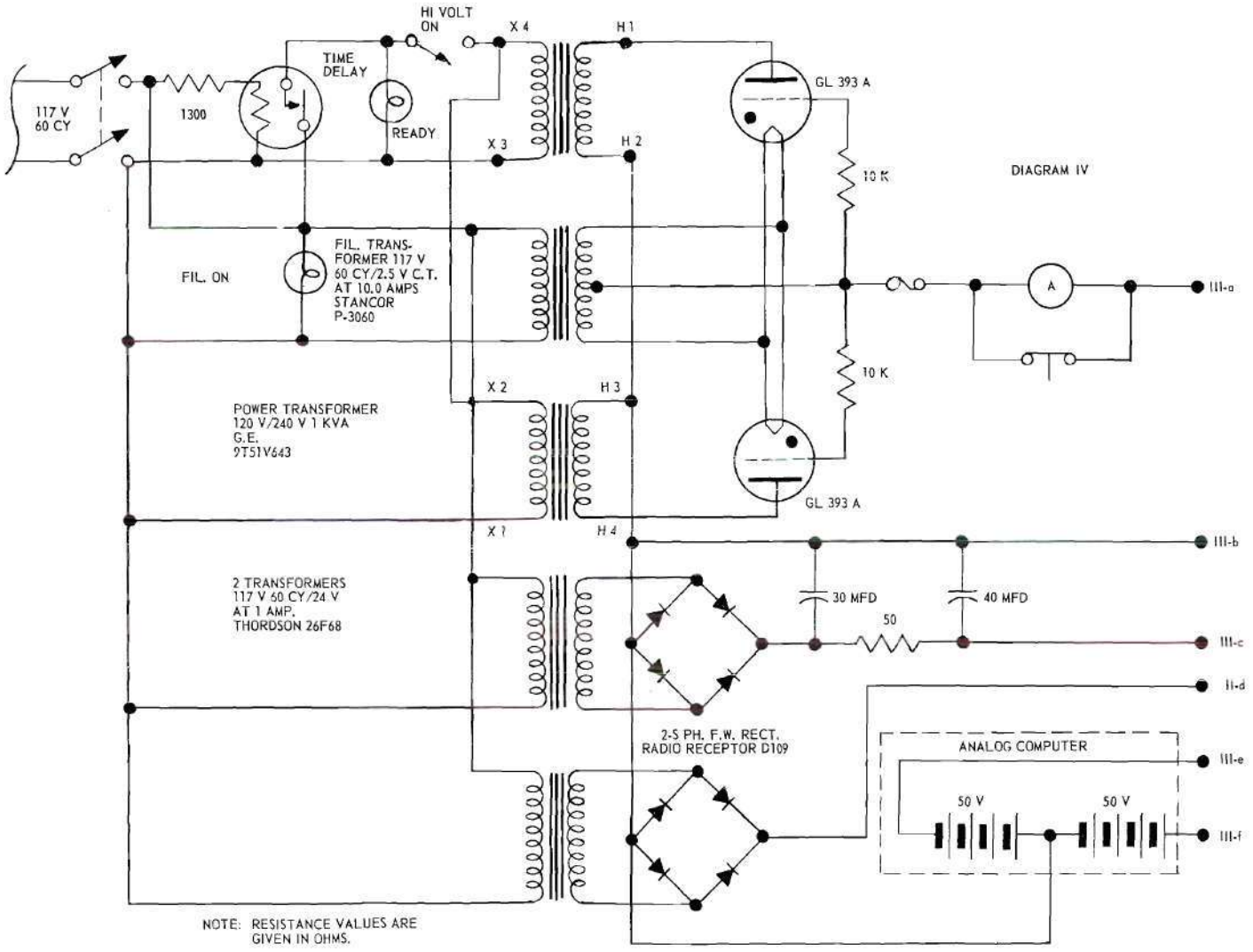

Figure 33. Power Supply Circuits.

APPENDIX B

EXPERIMENTAL DATA USED IN DETERMINING SYSTEM CONSTANTS

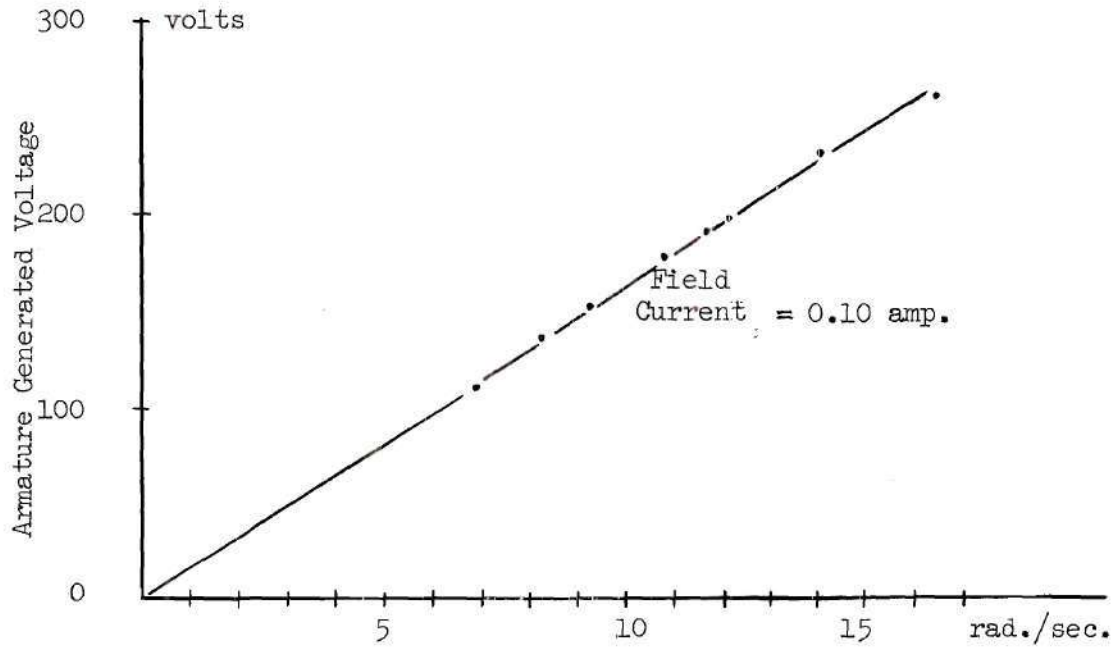

Fig. 34 Motor Generated Voltage Characteristic

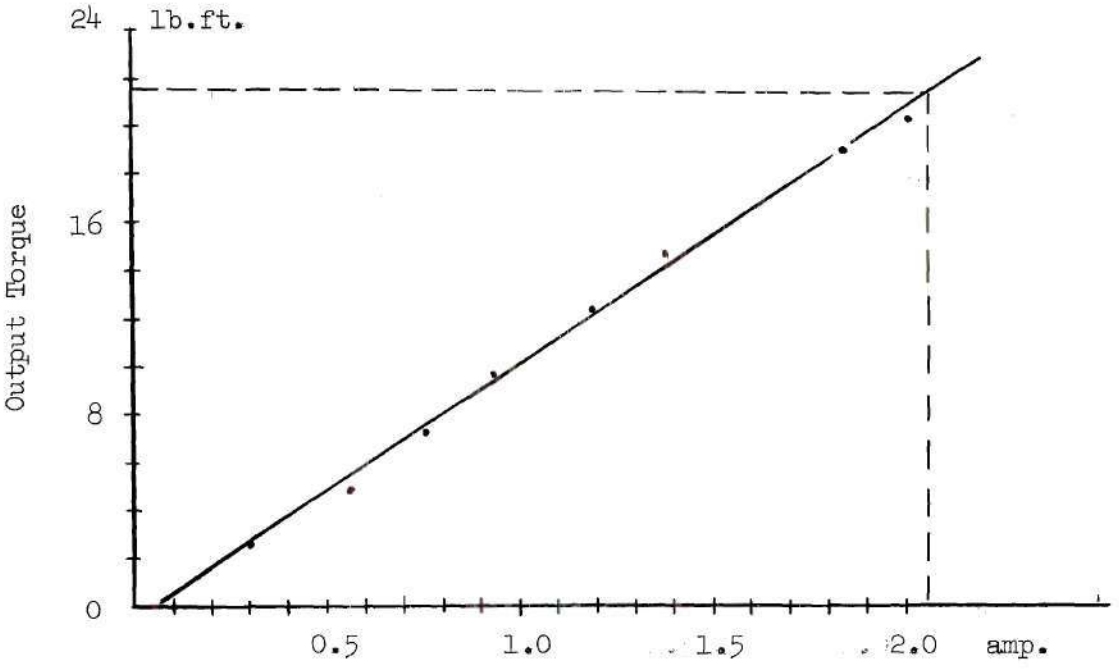

Fig. 35 Motor Torque Characteristic

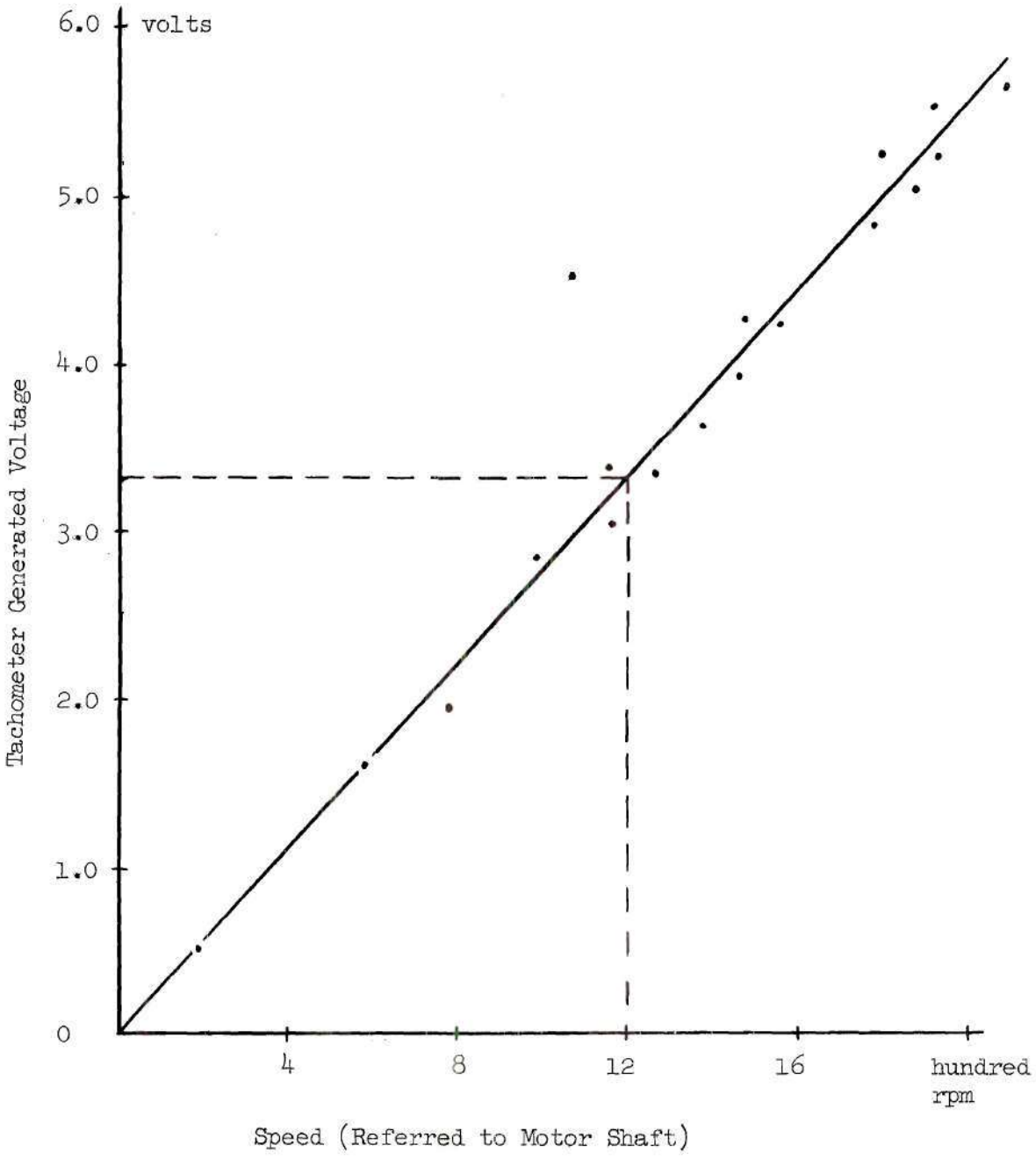

Fig. 36 Tachometer Generated Voltage Characteristic

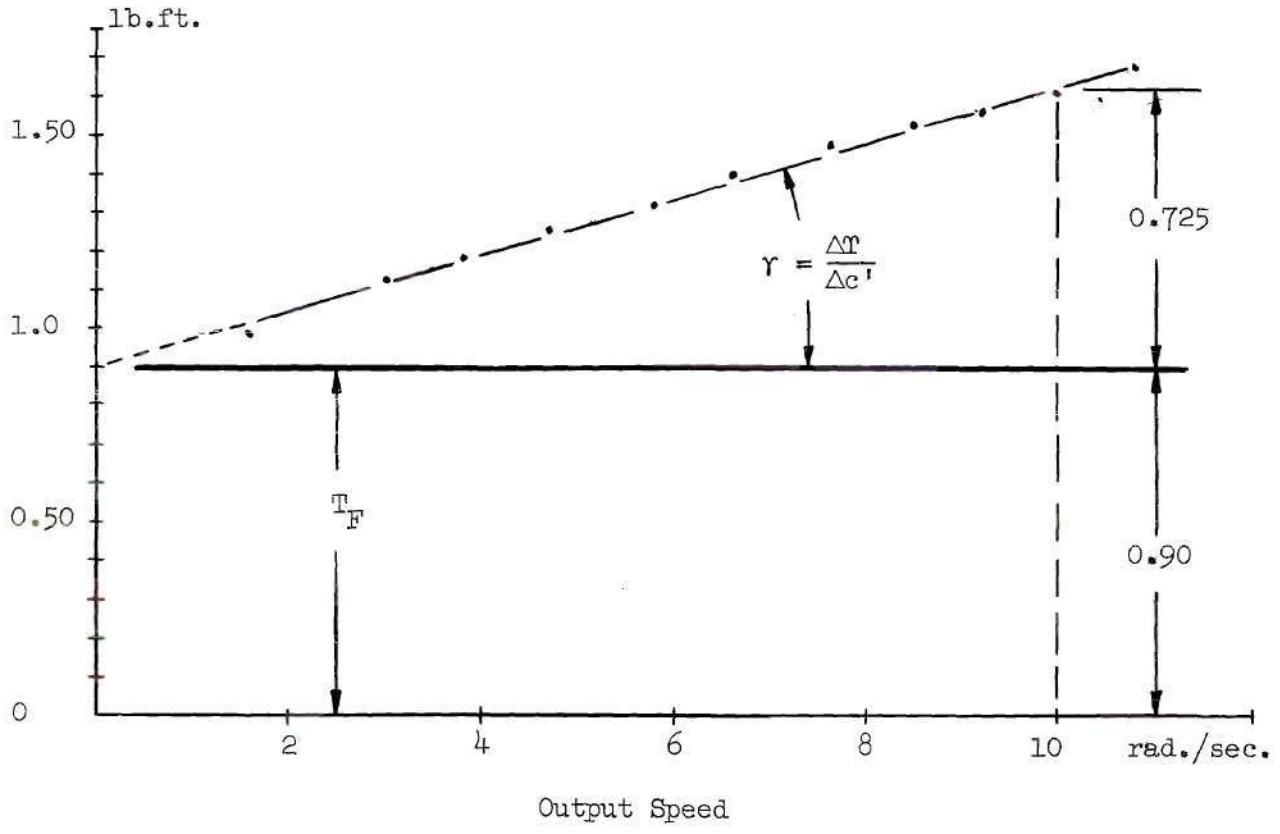

Fig. 37 Torque Developed for Several Constant Speeds

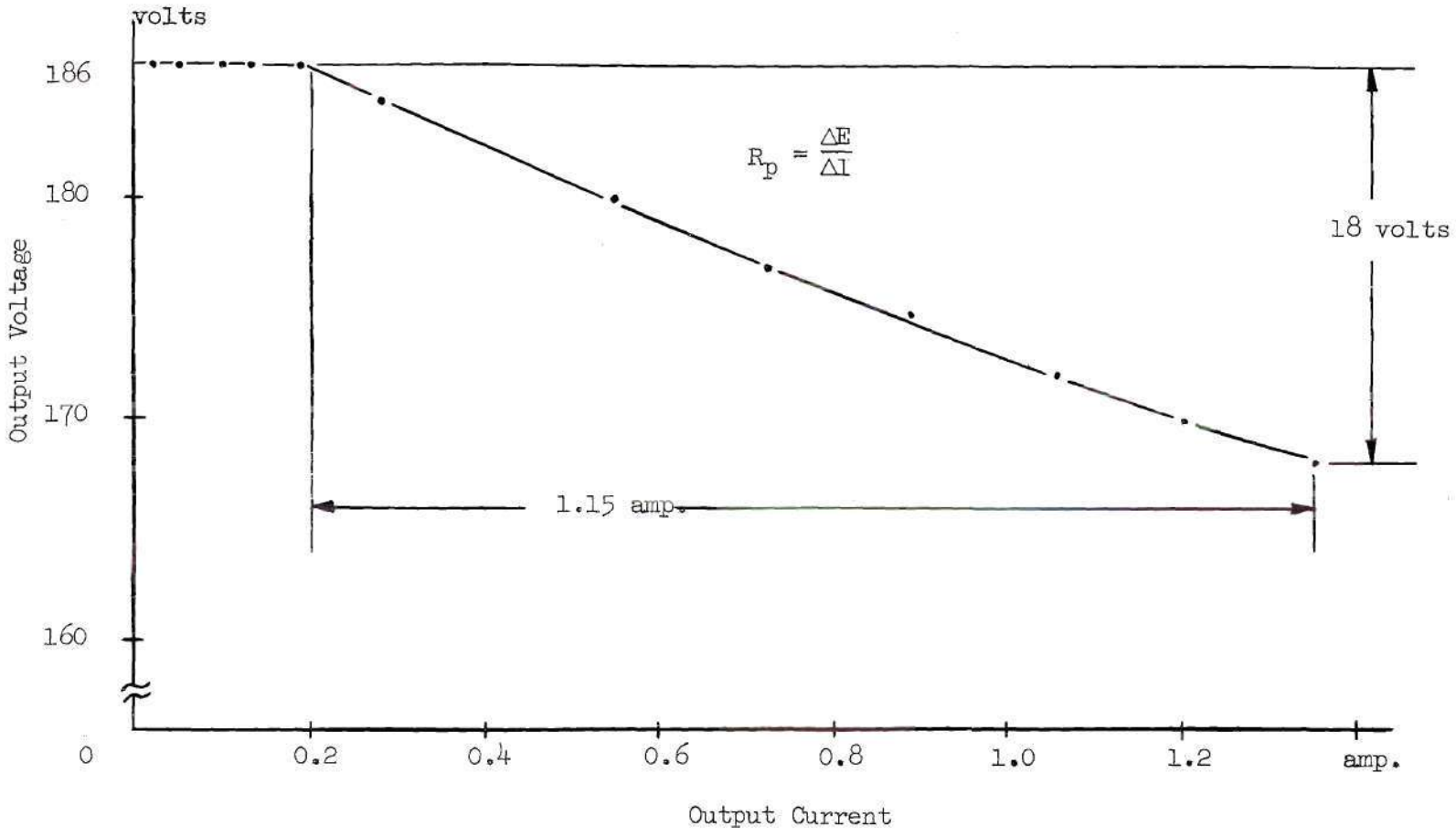

Fig. 38 Load Test of the Power Supply

Table 1. Determination of Series Field Resistance, R_s

I_a	Voltage Drop	R_s
0.091	0.20	2.20
0.103	0.25	2.17
0.110	0.27	2.46
0.118	0.30	2.54
0.125	0.35	2.80
0.131	0.37	2.82
0.138	0.39	2.82
0.142	0.40	2.82
0.145	0.40	2.75
0.150	0.40	2.65
0.157	0.40	2.53
Average		2.60

Table 2. Determination of Brush, Interpole, and Winding Resistance, R_a

I_a	Armature Voltage	R_a
0.038	0.60	15.70
0.050	1.00	20.00
0.080	1.50	18.70
0.105	2.39	22.70
0.118	2.60	22.00
0.125	2.70	21.60
0.138	2.90	21.00
0.170	3.20	18.70
Average		20.05

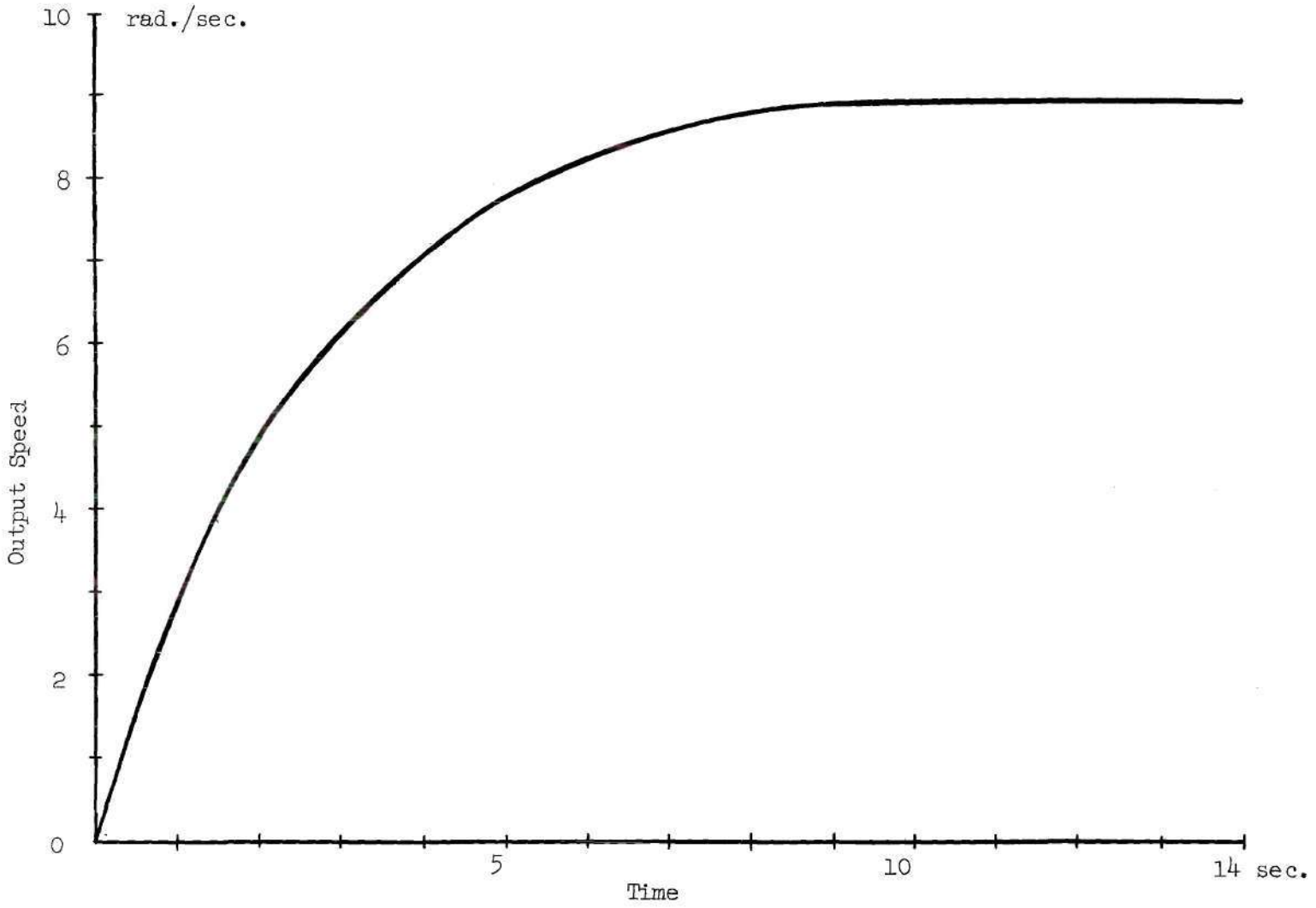

Fig. 39 Acceleration Test, Linear Scale

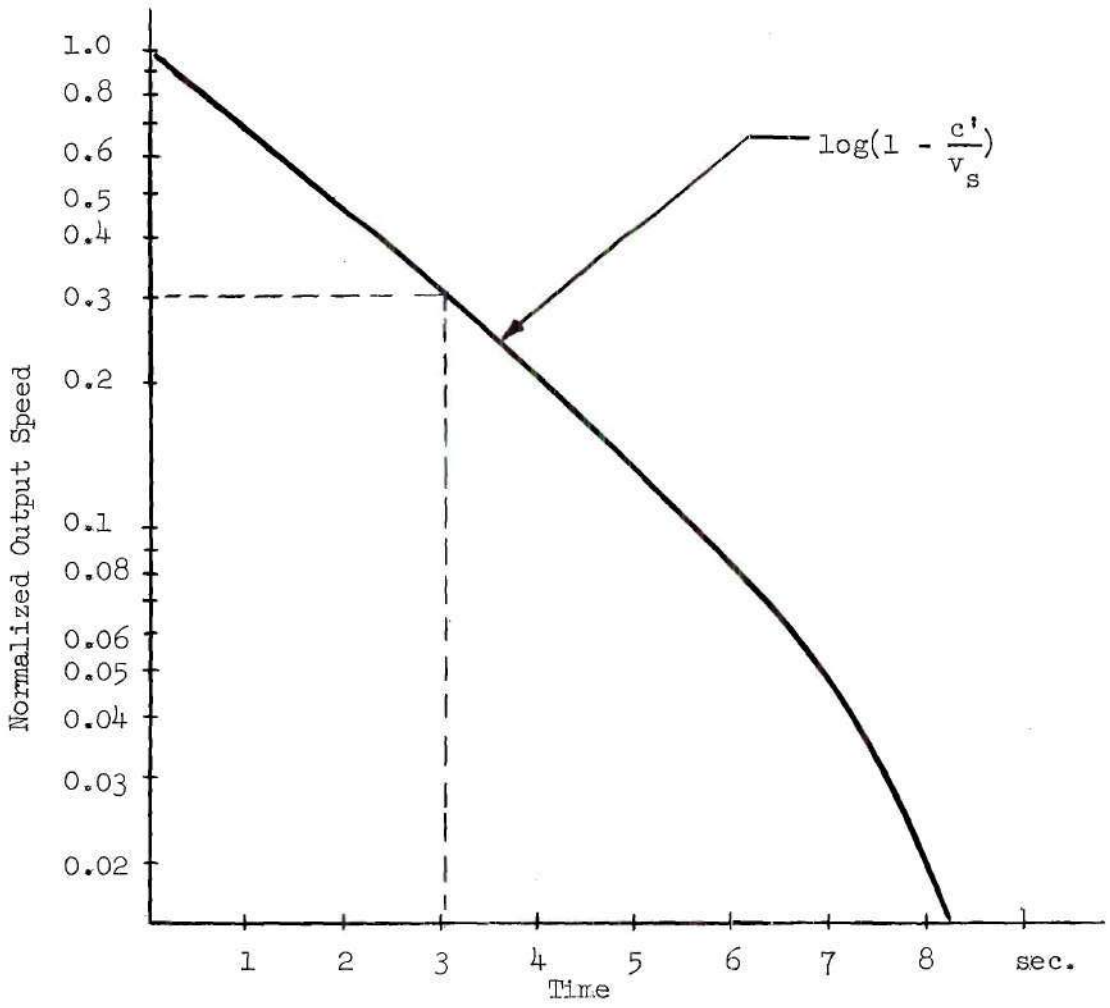

Fig. 40 Acceleration Test, Log Scale

APPENDIX C

NUMERICAL RESPONSE DATA

Table 3. Calculated Open Loop Trajectory for Negative x'

(Refer to Figs. 9 and 20)

x'	(1-x')	ln(1-x)	x'+ln(1-x')	x
-1.000	2.000	0.693	-0.307	0.307
-0.950	1.950	0.668	-0.282	0.282
-0.900	1.900	0.642	-0.258	0.258
-0.850	1.850	0.615	-0.235	0.235
-0.800	1.800	0.588	-0.212	0.212
-0.750	1.750	0.560	-0.190	0.190
-0.700	1.700	0.531	-0.169	0.169
-0.650	1.650	0.501	-0.149	0.149
-0.600	1.600	0.470	-0.130	0.130
-0.550	1.550	0.438	-0.112	0.112
-0.500	1.500	0.405	-0.095	0.095
-0.450	1.450	0.371	-0.079	0.079
-0.400	1.400	0.336	-0.064	0.064
-0.350	1.350	0.300	-0.050	0.050
-0.300	1.300	0.262	-0.038	0.038
-0.250	1.250	0.223	-0.027	0.027
-0.200	1.200	0.182	-0.018	0.018
-0.150	1.150	0.140	-0.010	0.010
-0.100	1.100	0.095	-0.005	0.005
-0.005	1.050	0.049	-0.001	0.001

Table 4. Calculated Open Loop Trajectory for Positive x'

(Refer to Figs. 9 and 20)

x'	(1-x')	ln(1-x')	x'+ln(1-x)	x
0.000	1.000	0.000	0.000	0.000
0.050	0.950	-0.051	-0.001	0.001
0.100	0.900	-0.105	-0.005	0.005
0.150	0.850	-0.162	-0.012	0.012
0.200	0.800	-0.223	-0.023	0.023
0.250	0.750	-0.288	-0.038	0.038
0.300	0.700	-0.357	-0.057	0.057
0.350	0.650	-0.431	-0.081	0.081
0.400	0.600	-0.511	-0.111	0.111
0.450	0.550	-0.598	-0.148	0.148
0.500	0.500	-0.693	-0.193	0.193
0.550	0.450	-0.798	-0.248	0.248
0.600	0.400	-0.916	-0.316	0.316
0.650	0.350	-1.050	-0.400	0.400
0.700	0.300	-1.204	-0.504	0.504
0.750	0.250	-1.386	-0.636	0.636
0.800	0.200	-1.609	-0.809	0.809
0.850	0.150	-1.897	-1.047	1.047
0.900	0.100	-2.302	-1.402	1.402
0.950	0.050	-2.995	-2.045	2.045

Table 5. Observed Open Loop Trajectory

(Refer to Fig. 17)

e	e'	e'
0.0	0.00	0.00
0.5	1.40	-2.20
1.0	2.60	-3.30
1.5	3.10	-4.20
2.0	3.40	-5.00
2.5	3.70	-6.00
3.0	4.00	-6.70
3.5	4.30	-7.20
4.0	4.60	-7.90
4.5	4.80	-8.30
5.0	5.00	-9.00
6.0	5.40	--
7.0	5.80	--
8.0	6.00	--
9.0	6.20	--
10.0	6.40	--
12.0	7.00	--
14.0	7.40	--
19.0	8.00	--
25.0	8.50	--

Table 6. Observed Open Loop Trajectory
Non-Dimensionalized

(Refer to Figs. 17 and 20)

x	e	e'	x'	e'	x'
0.050	1.11	2.70	0.312	- 3.70	- 0.413
0.100	2.23	3.60	0.403	- 5.30	- 0.593
0.150	3.34	4.10	0.458	- 6.90	- 0.790
0.200	4.46	4.80	0.537	- 8.30	- 0.927
0.250	5.57	5.20	0.580	-10.00	- 1.120
0.300	6.70	5.60	0.625	---	---
0.350	7.80	5.90	0.659	---	---
0.400	8.92	6.20	0.694	---	---
0.450	10.00	6.50	0.726	---	---
0.500	11.10	6.70	0.479	---	---
0.550	12.22	7.00	0.783	---	---
0.600	13.37	7.20	0.804	---	---
0.650	14.48	7.40	0.826	---	---
0.700	15.60	7.60	0.850	---	---
0.750	16.70	7.80	0.870	---	---
0.800	17.80	7.90	0.884	---	---
0.850	18.90	8.00	0.894	---	---
0.900	20.00	8.10	0.905	---	---
1.000	22.23	8.30	0.927	---	---
1.500	33.40	8.80	0.984	---	---

Table 7. Calculated Time Response, Displacement Input

(Refer to Fig. 21-a)

Displacement Input: 12.60 rad.
Initial Velocity: 0.00 rad./sec.

k = − 1

e(t)	x	x'	$(1+x')^{-1}$	$\ln(1+x')^{-1}$	p	0.565-x
12.60	0.565	-0.000	1.000	0.000	0.000	0.000
12.00	0.538	-0.210	1.265	0.235	0.235	0.027
11.00	0.493	-0.325	1.480	0.392	0.392	0.072
10.00	0.438	-0.420	1.720	0.542	0.542	0.127
9.00	0.403	-0.465	1.870	0.626	0.676	0.162
8.00	0.358	-0.520	2.080	0.732	0.732	0.207
7.00	0.313	-0.445	2.250	0.811	0.811	0.252
6.00	0.269	-0.592	2.450	0.896	0.896	0.296
5.00	0.224	-0.620	2.630	0.967	0.967	0.341
4.00	0.179	-0.650	2.860	1.051	1.051	0.386
3.58	0.160	-0.660	2.940	1.078	1.078	0.405

k = + 1

e(t)	x	x'	$\frac{1.660}{1-x'}$	$\ln(\frac{1.660}{1-x'})$	p	0.565-x
3.58	0.160	0.660	1.000	0.000	1.078	0.405
3.00	0.135	0.640	1.010	0.010	1.088	0.430
2.50	0.112	0.560	1.063	0.062	1.140	0.453
2.00	0.089	0.500	1.105	0.100	1.178	0.476
1.50	0.067	0.430	1.160	0.148	1.226	0.498
1.00	0.048	0.360	1.220	0.199	1.277	0.517
0.50	0.022	0.240	1.340	0.293	1.371	0.543
0.00	0.000	0.130	1.470	0.385	1.463	0.565
-0.25	-0.010	0.000	1.660	0.506	1.584	0.575

Table 8. Observed Time Response, Displacement Input

(Refer to Figs. 21-a and 22)

Displacement Input: 12.60 rad.
Initial Velocity: 0.00 rad./sec.

e(t)	e'(t)	x	x'	p
12.60	0.00	0.565	0.000	0.000
12.00	-2.00	0.538	0.223	0.235
11.00	-3.30	0.493	0.368	0.392
10.00	-4.00	0.438	0.447	0.520
9.00	-4.60	0.403	0.514	0.592
8.00	-5.10	0.358	0.570	0.665
7.00	-5.60	0.313	0.626	0.740
6.00	-5.91	0.269	0.659	0.814
5.00	-6.20	0.224	0.693	0.876
4.50	-6.30	0.179	0.704	0.920
4.00	-6.40	0.160	0.715	0.941
3.50	-6.45	0.157	0.720	0.960
3.00	-6.50	0.134	0.726	0.990
2.50	-6.60	0.112	0.738	1.010
2.00	-6.10	0.089	0.682	1.050
1.50	-5.50	0.067	0.615	1.090
1.00	-4.90	0.048	0.547	1.110
0.50	-3.60	0.022	0.402	1.190
0.00	-2.20	0.000	0.246	1.260
-0.25	0.00	-0.010	0.000	1.350

Table 9. Calculated Rime Response, Displacement Input and Initial Velocity

(Refer to Fig. 21-b)

Displacement Input: 12.60 rad.
Initial Velocity: 4.87 rad./sec.

k = - 1

e(t)	x	x'	$\frac{0.455}{1+x'}$	$\ln(\frac{0.455}{1+x'})$	p	0.565-x
12.60	0.565	0.545	1.000	0.000	0.000	0.000
12.00	0.538	0.560	1.035	0.034	0.034	0.027
11.00	0.493	0.590	1.110	0.104	0.104	0.072
10.00	0.438	0.630	1.240	0.215	0.215	0.127
9.00	0.403	0.650	1.300	0.262	0.262	0.162
8.00	0.358	0.675	1.400	0.336	0.336	0.207
7.00	0.313	0.695	1.494	0.402	0.402	0.252
6.00	0.269	0.710	1.570	0.451	0.451	0.296
5.00	0.223	0.730	1.685	0.521	0.521	0.342
3.77	0.169	0.750	1.820	0.599	0.599	0.396

k = + 1

e(t)	x	x'	$\frac{1.750}{1-x'}$	$\ln(\frac{1.750}{1-x'})$	p	0.565-x
3.77	0.169	0.750	1.000	0.000	0.599	0.396
3.00	0.134	0.650	1.060	0.058	0.657	0.431
2.50	0.112	0.575	1.110	0.104	0.703	0.453
2.00	0.089	0.500	1.166	0.153	0.752	0.476
1.50	0.067	0.430	1.222	0.200	0.799	0.498
1.00	0.048	0.360	1.288	0.253	0.852	0.517
0.50	0.022	0.245	1.405	0.340	0.939	0.543
0.00	0.000	0.120	1.562	0.446	1.045	0.565
0.25	0.010	0.000	1.750	0.560	1.159	0.575

Table 10. Observed Time Response, Displacement Input and Initial Velocity

(Refer to Figs. 21-b and 23)

Displacement Input: 12.60 rad.
Initial Velocity: 4.87 rad./sec.

e(t)	e'(t)	x	x'	p
12.60	-4.87	0.565	0.545	0.000
12.00	-5.11	0.538	0.571	0.035
11.00	-5.33	0.493	0.607	0.105
10.00	-5.90	0.438	0.658	0.214
9.00	-6.18	0.403	0.690	0.260
8.00	-6.47	0.358	0.722	0.357
7.00	-6.73	0.313	0.752	0.390
6.00	-7.00	0.269	0.781	0.445
5.00	-7.18	0.224	0.803	0.500
4.00	-7.39	0.179	0.826	0.550
3.60	-7.44	0.161	0.832	0.570
3.00	-7.30	0.134	0.816	0.600
2.50	-6.80	0.112	0.760	0.632
2.00	-6.00	0.089	0.672	0.670
1.50	-5.41	0.067	0.604	0.718
1.00	-4.80	0.048	0.547	0.755
0.50	-3.91	0.022	0.437	0.800
0.00	-2.89	0.000	0.324	0.850
-0.25	-0.00	0.010	0.000	1.000

APPENDIX D

CALCULATIONS

Determination of the tachometer constant:

From Fig. 36,

$$\frac{\text{Tach. generated emf}}{\text{Motor speed}} = \frac{3.25 \text{ volt}}{1200 \text{ rpm}}$$

$$= 0.00271 \frac{\text{volt}}{\text{rpm}}$$

From Fig. 29,

$$n = \frac{248}{15}$$

From Fig. 30,

$$\text{Amplification} = 5 \frac{\text{volt}}{\text{volt}}$$

Therefore referred to the output shaft and the x-y recorder,

$$K_d = (5 \frac{\text{volt}}{\text{volt}})(\frac{248}{15})(0.0027 \frac{\text{volt min.}}{\text{rev.}})(60 \frac{\text{sec.}}{\text{min.}})(\frac{1}{2\pi} \frac{\text{rev.}}{\text{rad.}})$$

$$K_d = 2.140 \frac{\text{volt sec.}}{\text{rad.}}$$

Determination of x-y recorder scale factors

From Fig. 32,

$$\text{Potentiometer output} = 5 \frac{\text{volt}}{\text{rev.}}$$

From Fig. 30,

$$\text{Amplification} = 1.5 \frac{\text{volt}}{\text{volt}}$$

x-input sensitivity: 75 volts = 15 in.

$$K_x = (5 \frac{\text{volt}}{\text{rev.}})(\frac{1}{2\pi} \frac{\text{rev.}}{\text{rad.}})(1.5 \frac{\text{volt}}{\text{volt}})(\frac{15}{75} \frac{\text{in.}}{\text{volt}})$$

$\therefore \quad K_x = 0.238 \frac{\text{in.}}{\text{rad.}}$

y-input sensitivity: 50 volts = 10 in.

$$K_y = (K_d)(\frac{10}{50} \frac{\text{in.}}{\text{volt}})$$

$$K_y = (2.140 \frac{\text{volt sec.}}{\text{rad.}})(\frac{10}{50} \frac{\text{in.}}{\text{volt}})$$

$\therefore \quad K_y = 0.428 \frac{\text{in.sec.}}{\text{rad.}}$

Generated emf constant:

From Fig. 34,

$$K_b = \frac{\Delta E}{\Delta c'} = (\frac{245}{15} \frac{\text{volt sec.}}{\text{rad.}})$$

$\therefore \quad K_b = 16.35 \frac{\text{volt sec.}}{\text{rad.}}$

Torque constant:

From Fig. 35,

$$\frac{\Delta T}{\Delta I_a} = \frac{21.5}{2} \frac{\text{lb.ft.}}{\text{amp.}}$$

$$\therefore \quad K_T = 10.7 \frac{\text{lb.ft.}}{\text{amp.}}$$

Viscous friction coefficient:

From Fig. 37,

$$\gamma = \frac{\Delta T}{\Delta c'} = \frac{0.725}{10} \frac{\text{lb.ft.sec.}}{\text{rad.}}$$

$$\therefore \quad \gamma = 0.0725 \frac{\text{lb.ft.sec.}}{\text{rad.}}$$

Dry friction torque:

From Fig. 37,

$$T_F = 0.90 \text{ lb.ft.}$$

Power supply resistance:

From Fig. 38,

$$R_p = \frac{\Delta E}{\Delta I} = \frac{18.0}{1.15} \frac{\text{volt}}{\text{amp.}}$$

$$\therefore \quad R_p = 15.6 \text{ ohms}$$

Power supply voltage: $E_p = 200$ volts

Series field resistance:

From Table 1,

$$R_s = 2.60 \text{ ohms}$$

Brush, interpole and winding resistance:

From Table 2,

$$R_a = 20.05 \text{ ohms}$$

Added armature resistance:

From Fig. 32,

$$R_d = 333.3 \text{ ohms}$$

Shunt conductance:

From (43), Chapter V,

$$G = (R_a + R_d + R_p + R_s)^{-1}$$

$$G = (371.6)^{-1}$$

$$\therefore \quad G = 0.00271 \ \frac{\text{amp.}}{\text{volt}}$$

Equivalent applied torque:

From (50), Chapter IV,

$$T = K_T G E_p$$

$$T = (10.7 \frac{\text{lb.ft.}}{\text{amp.}})(0.00271 \frac{\text{amp.}}{\text{volt}})(200 \text{ volt})$$

$$\therefore \quad T = 5.80 \text{ lb.ft.}$$

From Fig. 37,

$$T_F = 0.90 \text{ lb.ft.}$$

so that during acceleration,

$$T = (5.80 - 0.90) \text{ lb.ft.}$$

$$\therefore \quad T = 4.90 \text{ lb.ft.}$$

Total viscous coefficient:

From (49), Chapter IV,

$$f = \gamma + GK_T K_b$$

$$f = (0.0725 \frac{\text{lb.ft.sec.}}{\text{rad.}}) + (0.00271 \frac{\text{amp.}}{\text{volt}})(10.7 \frac{\text{lb.ft.}}{\text{amp.}})(16.35 \frac{\text{volt sec.}}{\text{rad.}})$$

$$f = (0.0725 + 0.474)(\frac{\text{lb.ft.sec.}}{\text{rad.}})$$

$$\therefore \quad f = 0.547 \frac{\text{lb.ft.sec.}}{\text{rad.}}$$

Time constant:

From Fig. 40, linear portion of the curve,

$$t = 3 \text{ sec.}$$

and

$$(1 - \frac{c'}{v_s}) = 0.3$$

From (63), Chapter V,

$$q = \frac{-t}{\ln(1 - \frac{c'}{v_s})}$$

$$q = \frac{-3.00}{\ln 0.3} \text{ sec.}$$

$$q = \frac{-3.00}{-1.204} \text{ sec.}$$

$$\therefore \quad q = 2.49 \text{ sec.}$$

Total polar moment of inertia:

From (64), Chapter V,

$$J = qf$$

$$J = (2.49 \text{ sec.})(0.547 \frac{\text{lb.ft.sec.}}{\text{rad.}})$$

$$J = 1.36 \frac{\text{lb.ft.sec.}^2}{\text{rad.}}$$

or

$$J = 1.36\left(\frac{\text{lb.ft.}}{\text{sec.}^2}\right)(\text{ft.sec.}^2)$$

$$\therefore \quad J = 1.36 \text{ lb.ft.}^2$$

Saturation velocity:

From (53), Chapter IV,

$$v_s = \frac{T}{f}$$

$$v_s = \left(\frac{4.90}{0.547}\right)\left(\frac{\text{lb.ft.rad.}}{\text{lb.ft.sec.}}\right)$$

$$v_s = 8.95 \ \frac{\text{rad.}}{\text{sec.}}$$

Table 6:

For a selected value of x, e.g.,

$$x = 0.450$$

The corresponding value of e is given by

$$e = q \, v_s \, x$$

$$e = (2.49 \text{ sec.})\left(8.95 \ \frac{\text{rad.}}{\text{sec.}}\right)(0.450)$$

$$e = 10.0 \text{ rad.}$$

From Fig. 17, Chapter V, the coordinate value of e' for e = 10.0 is

$$e' = 6.50$$

for which

$$x' = \frac{e'}{v_s}$$

$$\therefore \quad x' = \frac{6.50}{8.95} = 0.726 \ .$$

Tables 3 and 4:

From (28), Chapter III,

If k = + 1

$$x = - [x' + \ln(1-x')]$$

If x' = + 0.500,

$$x = - [0.500 + \ln 0.500]$$

$$x = - [0.500 - 0.693]$$

$$\therefore \quad x = + 0.193$$

If x' = - 0.500,

$$x = - [- 0.500 + \ln 1.500]$$

$$x = - [- 0.500 + 0.405]$$

$$\therefore \quad x = 0.095$$

Tables 7 and 9:

From (25), Chapter III,

$$p = \ln \left(\frac{k - x'_o}{k - x'}\right)$$

For

$k = - 1$

$x'_o = - 0.545$

$x' = 0.590$

$$p = \ln \left(\frac{0.455}{0.410}\right)$$

$$p = \ln 1.110$$

$\therefore$ $p = 0.104.$

For

$k = + 1$

$x'_o = - 0.750$

$x' = - 0.575$

$p_o = 0.599$

$$p = \ln \left(\frac{1.750}{1.575}\right) + 0.599$$

$$p = \ln 1.110 + 0.599$$

$$\therefore \quad p = 0.703.$$

BIBLIOGRAPHY

BIBLIOGRAPHY

Literature Cited

1. Thaler, G. J. and R. G. Brown, Servomechanism Analysis, New York: McGraw-Hill Book Company, Inc., 1953.

2. Truxal, J. G., Automatic Feedback Control System Synthesis, New York: McGraw-Hill Book Company, Inc., 1955.

3. Hazen, H. L., "Theory of Servo-mechanisms," Journal of The Franklin Institute, 218 (Sept. 1934), pp. 279-331.

4. DeJuhasz, K. J., "Discussion of Paper, 'Forced and Free Motion of a Mass on an Air Spring,'" Journal of Applied Mechanics, 12 (Sept. 1945), pp. A-175-177.

5. Minorsky, N., "On Parametric Excitation," Journal of The Franklin Institute, 240 (July 1945), pp. 25-46.

6. Andronow, A. A. and C. E. Chaikin, Theory of Oscillations, Moscow, 1937; English edition, Solomon Lefschetz, Princeton, New Jersey: Princeton University Press, 1949.

7. MacColl, L. A., Fundamental Theory of Servomechanisms, Princeton New Jersey: D. Van Nostrand Company, Inc., 1945. (See Appendix)

8. Weiss, H. K., "Analysis of Relay Servomechanisms," Journal of The Aeronautical Sciences, 13 (July 1946), pp. 364-76.

9. Flügge-Lotz, I., Discontinuous Automatic Control, Princeton, New Jersey: Princeton University Press, 1953.

10. MacDonald, D., "Non Linear Techniques for Improving Servo Performance," Proceedings of the National Electronics Conference, Chicago, Illinois, September 1950 (April 1951), pp. 400-421.

11. Hopkin, A. M., "A Phase Plane Approach to the Compensation of Saturating Servomechanisms," Transactions AIEE, 72, Part I (1951), pp. 631-639.

12. Bogner, I. and L. F. Kazda, "An Investigation of Switching Criteria for Higher Order Servo Mechanisms," Transactions AIEE, Applications and Industry, 13 (July 1954), pp. 118-127.

13. Kendall, P. E., and I. Bogner, "Research in Nonlinear Mechanics as Applied to Servomechanisms," WADC Technical Report, 53-521, Cook Electric Company, 1953.

14. Op. Cit., p. 613.

15. Kochenburger, R. J., "Frequency Response Method for Synthesizing and Analyzing Contactor Servomechanisms," Transactions AIEE, 69, Part I (1950), pp. 20-83.

16. Loc. Cit.

17. Loc. Cit.

18. Loc. Cit.

19. Loc. Cit.

Other References

20. Cosgriff, R. L., Nonlinear Control Systems, New York: McGraw-Hill Book Company, Inc., 1958.

21. Silva, L. M., "Nonlinear Optimization of Relay Servomechanisms," University of California (Berkeley), Electronics Research Laboratory Report, 106, Ser. 60, April 15, 1954.

22. Smith, O. M., Control Systems Engineering, New York: McGraw-Hill Book Company, Inc., 1958.